Oxygen isotope shifts reveal fluid-fluxed melting in continental anatexis

Check for updates

Silvia Volante [1,2] ✉, Amaury Pourteau[1], Zheng-Xiang Li [1,3], William J. Collins [1], Luc S. Doucet [1], Hugo K. H. Olierook [4], Laure Martin[5] & Matthijs A. Smit [6,7]

Fluid-flux melting is increasingly recognised as a key mechanism for continental crust growth and recycling, but the abundance and sources of the external fluids involved in this process are typically uncertain. Here we use zircon and garnet oxygen isotope data, geochronology, and petrological analysis of mid- to lower-crustal rocks from the Georgetown Inlier, Australia, to explore the composition and origin of anatexis-triggering fluids. Tonalite veins and garnetite residues show higher zircon $\delta^{18}O$ values (~6‰) than their amphibolite source (~2–3‰), whereas sediment-derived granites show lower values (6‰) than those of typical siliciclastic sources (10–20‰). Mass balance modelling suggests that these isotopic shifts result from the interaction with mantle-derived fluids. Asthenospheric mantle upwelling beneath the Georgetown crust during slab rollback or break-off provided heat and fluids, generating hydrous mafic underplates that exsolved mantle-derived water, promoting crustal anatexis. This process may have been key in shaping Earth's early buoyant sodic continental crust.

The presence of water on Earth is intrinsically linked to the unique characteristics of our planet, including the development of a buoyant felsic continental crust and the dynamic processes of plate tectonics, phenomena absent on other planetary bodies. The formation and recycling of continental crust require a delicate balance between heat and water availability[1]. Substantial heat sources, such as radioactive decay of specific elements enriched in felsic rocks, magmatic intrusions, and deep mantle upwelling beneath the continental crust, are well documented[2]. However, the sources and pathways of water within the crust are less clearly defined.

Continental crust production and recycling have primarily been attributed to dehydration melting—the breakdown of hydrous minerals (amphibole, biotite, muscovite) in high-grade metamorphic rocks at temperatures above 750 °C[3]. In recent years, fluid-present melting has been recognised as a viable alternative to explain the low magmatic temperature estimates observed in felsic rocks globally[1,4–6]. This process accounts for significant degrees of partial melting of metamorphic rocks below 800 °C[5,7], and generation of a substantial amount of sodic crust in the early Earth[8] along with more evolved, calc-alkaline I-type granites and adakite in the Proterozoic and Phanerozoic[9–12]. The critical role of water in continental

crust formation has been explored since the 1950s through petrological experiments, which demonstrated that the presence of fluids in any rock type lowers the solidus temperature and increases the melt fraction[13]. Consequently, water-fluxed melting can generate higher melt volumes at lower temperatures than dehydration melting, which typically requires temperatures above 850 °C and is restricted to fertile rock compositions[3]. Several recent studies highlight the importance of fluids in forming large plutons at relatively low temperatures[4,14], and controlling crustal melting temperatures[5], residual mineral assemblages, and melt compositions[4,15] not only within Phanerozoic and Proterozoic convergent settings but also within Archaean environments. In younger orogens such as the Cordilleran, Lachlan or Adelaide Fold Belt, extensive work in the recent years demonstrated the critical role of water in producing hydrous underplating of arc basaltic magmas to generate juvenile continental crust, but also that water availability within different tectonic settings controls the production of compositionally diverse granitic magmas[5,6,9]. Other geochemical, petrological and thermodynamic modelling studies have documented water-flux melting in subduction-related settings to produce tonalite, I-type (calc-alkaline) and adakite magmas through partial melting of hydrous mafic

[1]Earth Dynamics Research Group, ARC Centre of Excellence for Core to Crust Fluid Systems (CCFS) and The Institute for Geoscience Research (TIGeR), School of Earth and Planetary Sciences, Curtin University, Perth, WA, Australia. [2]Structural Geology and Tectonics Group, Geological Institute, Department of Earth and Planetary Sciences, ETH Zürich, Zürich, Switzerland. [3]Earth Evolution and Dynamics Research Center (EDRC), Laoshan Laboratory, Qingdao, China. [4]John de Laeter Centre and Timescales of Mineral Systems Group, School of Earth and Planetary Sciences, Curtin University, Perth, WA, Australia. [5]Centre for Microscopy, Characterisation and Analysis, The University of Western Australia, Perth, WA, Australia. [6]Pacific Centre for Isotope and Geochemical Research, Department of Earth, Ocean and Atmosphere Sciences, University of British Columbia, Vancouver, BC, Canada. [7]Department of Geosciences, Swedish Museum of Natural History, Stockholm, Sweden. ✉e-mail: svolante@eaps.ethz.ch

crust and during late-collisional stages to produce more evolved potassic magmas by water-flux melting of mid- to lower-crustal material[11,12,16–19]. Crustal-scale shear zones within Proterozoic and Phanerozoic convergent settings have also been demonstrated to act as efficient pathways for fluid transfer, facilitating partial melting of different crustal levels[4,9,15,20]. Within Mesoproterozoic amphibolites from Gore Mountain, micrometric droplets of trondhjemitic melt found in garnet megacrysts also support fluid-flux melting of the hosting mafic gabbro at lower crustal conditions[21]. The important role of water as key ingredient to produce sodic felsic crust in the early Earth has also increasingly gathered more evidence, supporting water-flux melting as critical process for crustal growth within the first 2.0 billion years after the formation of our planet[22–25]. Advances in experimental petrology and phase equilibrium modelling reveal that fluid-fluxed melting should leave behind hydrous residues that are variably enriched in hornblende and/or garnet, based on their initial composition[9,26–29]. Therefore, in many terranes worldwide and through Earth history, water-flux melting has been increasingly identified as an important process for crustal growth.

Outstanding challenges associated with water-fluxed melting include (i) identifying potential fluid sources and (ii) understanding the flow mechanisms required to generate the large volumes needed for fluid saturation in possibly important regions of the continental crust[9]. However, identifying the fluid sources is mostly by inference, as much of the research has predominantly focused on granite compositions—both locally and globally—linking these granites to magmas extracted from often unexposed reservoirs.

The composition and possible origin of fluids during crustal melting can be evaluated using oxygen isotope compositions, which are sensitive to fluid-rock interaction processes[30–32]. Unlike whole-rock analyses, resilient mineral phases like zircon and garnet effectively retain their primary oxygen isotope signatures due to slow intracrystalline diffusion[33,34]. The oxygen isotope compositions of zircon in igneous rocks reflect those of the parental magma, enabling differentiation between various source candidates or assessment of geochemical alteration caused by isotopically distinct external fluids[19,24,35–37]. Garnet extends this analytical approach to Zr-undersaturated systems, although some fractional effects may occur, especially at lower garnet growth temperatures or with higher grossular content in garnet[38–41]. Recent studies have used oxygen isotope composition of detrital zircon and Monte Carlo simulations to distinguish crustal growth pulses in the Archaean and trace their interaction with fluids to explore the emergence of the hydrological cycles on the early Earth[37]. Light $\delta^{18}O$ values of zircon were interpreted as the result of interaction of emerged continents with fresh water and the start of the hydrological cycle on Earth[37]. Combined with other studies using oxygen isotope composition of zircon[19,24,42,43], these works highlight the efficacy of using oxygen isotopes to unravel the interaction of Precambrian rocks with primitive and/or primordial melt and fluid sources.

In this contribution, we use this isotope geochemistry-based tool to investigate fluid-fluxed processes in a well-exposed and well-preserved cross-section from the Proterozoic orogen in NE Australia, where field relationships between association of source rocks, melt products and restite occur. We describe a well-constrained mid- to lower crustal section (6–9 kbar) from the Georgetown Inlier, where fluid-fluxed melting of amphibolites and paragneisses has been previously suggested as important mechanism to produce tonalite and granitic melts, respectively, during 1550 Ma post-collisional extension[24,9,15,20,44]. Tonalitic sheets and veins are closely related to garnetite and minor hornblendite, which are interpreted as residues of in situ fluid-fluxed lower crustal melting[15,27,28]. To further test the occurrence of fluid-flux melting processes as dominant physicochemical mechanism for crustal growth, oxygen isotope analysis was applied to samples from the inlier. Only a heterogeneous isotopic signature between the source and the produced melt would support the hypothesis of ingress of external fluids to trigger partial melting of the mid and lower crust. If the latter is supported, the remaining question would be: did the fluids stem from the surrounding melting metasedimentary rocks or another, more cryptic source? We show that the oxygen isotope compositions of the granitoids significantly diverge from those of their respective host rock sources, converging towards a

distinctive mantle isotopic signature akin to that of contemporaneous garnetite (Fig. 1). Our fluid–rock interaction models support the interpretation that water-fluxed melting of amphibolite and paragneiss produced the Georgetown sodic and potassic melts but also required that the fluids involved were of mantle origin. This study highlights that, alongside dehydration melting of fertile lithologies, water-fluxed melting is an essential mechanism in continental growth and differentiation processes. These findings shed new light on the important role that water-fluxed melting by mantle-derived fluids may have played in producing most of the sodic felsic crust that formed the first building blocks of the Archaean cratons.

## Geological setting and rock relations

The upper amphibolite- to lower-granulite-facies domain of the eastern Georgetown Inlier represents the deep-crustal equivalents of a > 1700 to 1620 Ma stratigraphic succession of siliciclastic rocks with intercalated 1670–1650 Ma low-K, Fe-rich tholeiite lava flows and sills, which is exposed in the low-metamorphic-grade western domain[45,46] (Supplementary Fig. S1). Following collision-related burial and intermediate temperature/pressure (T/P) metamorphism at 1600–1590 Ma, the Georgetown Inlier underwent widespread anatexis and felsic magmatism between 1565 and 1540 Ma[47–50]. During this period, siliciclastic rocks experienced pervasive partial melting around 750–800 °C in the lower crust, potentially serving as the source for a voluminous coeval, syn-kinematic granitic complex emplaced at mid-crustal depths in the central domain. Coeval, felsic volcanic and sub-volcanic rocks emplaced at or near the surface in the western domain represent the upper-crust expression of this magmatic phase. A subordinate tonalite–trondhjemite–granodiorite (TTG) suite was emplaced in the middle crust, derived by partial melting of amphibolite[15,45]. Sediment-derived (S-type) and TTG plutons in the Georgetown Inlier have been regarded as low-temperature, hydrous igneous mushes derived through fluid-present melting of the lower-crustal metasedimentary and amphibolitic rocks, respectively[4,15]. Syn-magmatic formation of residual garnetite associated with tonalite veining was reported in the eastern domain, providing an opportunity to investigate the nature and timing of fluid infiltration and partial melting in the lower crust section of the orogen. Fluid flux during anatexis may have been facilitated by a crustal-scale detachment zone, juxtaposing the upper-, western crustal domain to the mid-to lower-crustal domains (Supplementary Fig. S1), and acting as network of pathways for fluid circulation during the post-collisional extensional stage at ca. 1550 Ma[44,51,52]. In contrast, drier and hotter granites originated in the lower crust and raised to upper crustal levels, interacting with domains of limited or absent flux activity.

In combination to petrological observations of magmatic and metamorphic samples (Supplementary Notes 1; Supplementary Data Tables S1 and S2 and Supplementary Fig. S2), we present geochronological data (Supplementary Data Table S3 and Supplementary Figs. S3 and S4) and in-situ oxygen isotope analyses (Supplementary Data Table S4 and Supplementary Figs. S3, S5 and S6) of zircon and garnet (Supplementary Data Table S5) from amphibolite gneiss (EIN1607, EIN1611), genetically related tonalite (ES07, ES31, EIN1702), and garnetite (ES34, ES36). Additionally, in-situ oxygen isotope compositions of zircon from previously dated c. 1555 Ma S-type granites and leucosomes[4] are presented (Supplementary Data Table S4). A complete list of all parameters used for the Monte Carlo simulations is included in Supplementary Data Table S6. A compilation of metasomatic and metamorphic garnet mineral chemistry is presented for the study area (Supplementary Data Table S7 and Supplementary Fig. S7).

Amphibolite and associated tonalite

Amphibolite in the eastern Georgetown Inlier (Fig. 1) consists of hornblende-rich, ilmenite-bearing gneiss comprising common clinopyroxene, occasional garnet (as in EIN1607 and EIN1611) and sparse orthopyroxene. In the field, compositional layering in mafic gneiss is observed as metre- to decimetre-scale variation of plagioclase-, garnet- and clinopyroxene- and hornblende-rich layers, with sparse leucocratic interstices of plagioclase and quartz. Partial melting of amphibolite has formed a continuum of

Fig. 1 | **Prominent outcrop-scale evidence of the partial melting features in the lower-crustal eastern domain of the Georgetown Inlier. A** Field evidence for in-situ partial melting of the amphibolite in the Einasleigh area generating tonalite sheets, network of tonalitic veins and isolated melt pockets. Inset: network of tonalite melt pockets and veins with diffuse contacts with the host rock. **B** In-situ partial melting of amphibolite and the produced tonalitic melt. Diffuse contacts between the veins and the host amphibolite. The host rock presents dilatant melt-rich patches merging into the investigated veins. **C** High degree of in-situ partial melting of the paragneiss. Inset: granitic leucosomes produced by in-situ partial melting. **D** In-situ partially melted amphibolite and associated tonalitic veins and dykes and garnet-rich garnetite. **E** Garnet-bearing metasomatic rock (garnetite) composed of garnet, clinopyroxene and subordinate quartz and plagioclase.
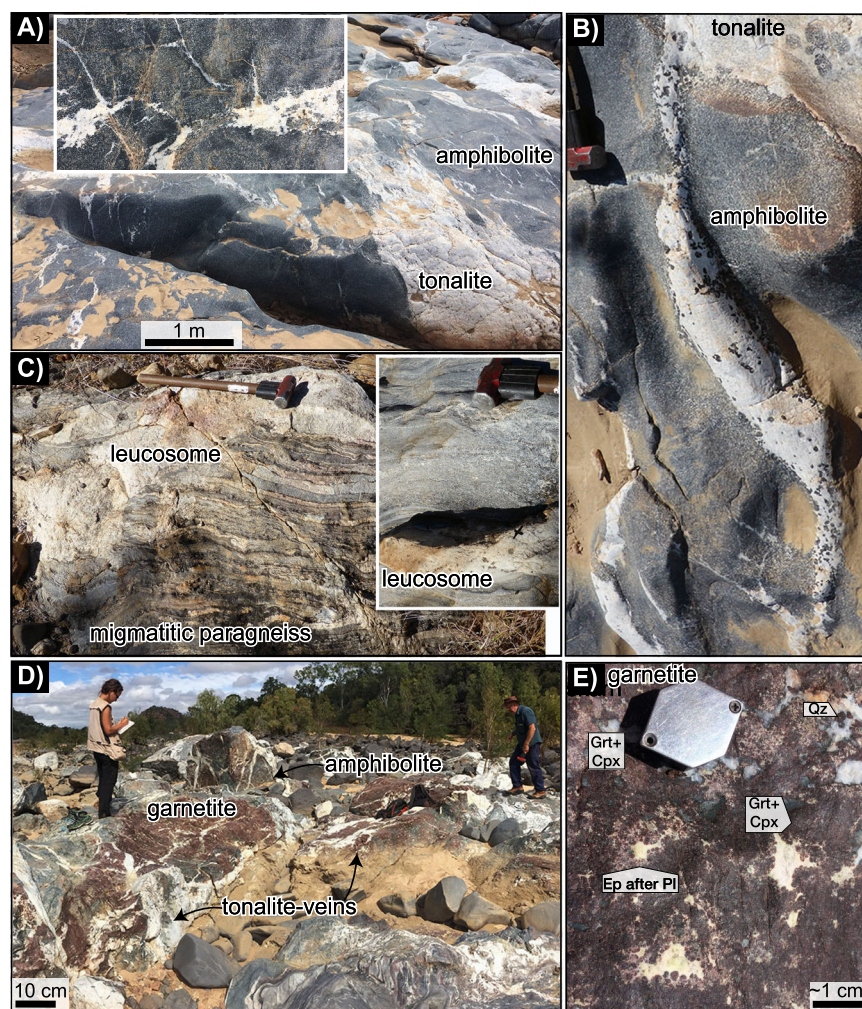
leucocratic domains at all scales: mm-scale films and layers adjacent to hornblende or garnet crystals connect to isolated cm- to- dm-sized, in-situ dilatant leucocratic patches and in-source veinlets that are sub-parallel or highly oblique to the gneissic fabric. These patches coalesce into dm-thick veins and cross-cutting dykes, up-to-m-thick (Fig. 1A, B). While partial melting appears incipient in some mafic rocks (in the northeastern domain), others show evidence of extensive partial melting and melt loss (in the southeastern domain; Fig. 1A, E). Melt fractions of c. 20–30% estimated by thermodynamic modelling[15], combined with widespread migmatitic textures and the production of leucosomes, support significant water-fluxed partial melting at the outcrop-scale. Leucosome pockets and veins have diffuse contacts with the host rocks and generally lack any spatial relationships with anhydrous peritectic minerals (Fig. 1A, B). Tonalite veins are primarily composed of plagioclase and quartz with common hornblende, occasional garnet (sample ES31) or biotite (mostly replaced by epidote and chlorite, as in ES07aV). Hornblende displays euhedral crystal edges with the leucocratic domains, where quartz is interstitial to sub-euhedral/automorphic plagioclase. Magma mingling is evident in well-developed tonalite veins, with pegmatitic, hornblende-bearing domains (sample ES07aV) derived from the local amphibolite and biotite-bearing domains (ES07aG). These features collectively support in-situ generation of significant amount of tonalitic melt in the exposed Georgetown lower-crustal rocks.

Sediment-derived (S-type) granitic rocks

The 1565–1540 Ma sediment-derived intrusions (i.e. S-type granites) in the central mid-crustal domain of the Georgetown Inlier consist of foliated,

biotite- and/or muscovite-bearing granite plutons and sheets (including sample RR75 and RR77) that were generated through water-fluxed melting at temperatures of ~730 °C[4]. Contemporaneous sub-volcanic granite (sample RR71) and comagmatic rhyolite (RR72) from the western domain are interpreted to have originated from hotter, drier magmas, produced preferentially through dehydration melting around and above 800 °C[4]. Granitic rocks of the upper crust domain were associated with similarly hot and dry magmas represented by in-source granitic leucocratic veins (ES19) in the eastern inlier.

Paragneiss layers in the eastern inlier display widespread partial melting features (Fig. 1C). Migmatite structures include stromatic metatexite, net-structured metatexite as well as schollen and nebulitic diatexite, representing variable degrees of melting. Leucocratic veins within the paragneiss predominantly have sharp contacts with the host rocks, and the network of leucocratic material displays variable appearances. These characteristics have been previously described as typical of dehydration-melting processes[9]. The extensive migmatisation textures from the eastern domain are estimated to have occurred at temperatures around 750–800 °C, with sparse peritectic garnet growth in the leucocratic portions indicating a drier or deeper lower crustal component[4,48]. In contrast, melt fractions of c. 30% estimated by thermodynamic modelling for the generation of low temperature (700–750 °C), hydrous S-type granites in the central domain suggest significant water-flux partial melting of the metasedimentary rocks at c. 1550 Ma[4]. This textural and petrological evidence indicates an alternation between melting of sedimentary rocks by pulsed influxes of aqueous fluids (central domain) and by local mica breakdown.

Results

The occurrence of fluid-fluxed melting as important physicochemical mechanism for crust formation in the Georgetown Inlier was previously proposed and is here tested via the application of in-situ oxygen isotope analysis of zircon and garnet from amphibolite, genetically related tonalite and restitic garnetite, and sediment-derived granitic rocks from the Georgetown Inlier. While the volcanic and subvolcanic rocks, S-type granite and the paragneiss leucosomes samples were collected from the western, central and eastern domains of the inlier, representing the upper, mid- and lower-crustal sections, respectively, samples for the mafic system come from the eastern, lower-crustal domain. Magmatic and metamorphic samples collected from spatially and temporally related amphibolite and tonalite veins (Fig. 1A, B) in the northern portion of the eastern domain reflect the incipient process of in-situ partial melting of the amphibolite, whereas the investigated tonalite sheets and garnetite from the southern part of the same domain are representative of more extensive melt production and restitic material (Fig. 1D, E). The eastern domain is a vast and poorly exposed region, with widespread but not ubiquitous tonalitic leucosomes production in the amphibolite along with rarely exposed garnet- and hornblende-bearing restitic portions. For these reasons, the analysed less melted amphibolite source and the restitic garnetite were found in variably melted portions of the same lower crustal level[15,48,49,53] and represent the best candidates to reflect the incipient and more evolved partial melting process, respectively.

Zircon and garnet O isotopes

Amphibolite and associated tonalite. Zircon from amphibolite yields $^{207}Pb/^{206}Pb$ weighted mean dates of 1553 ± 7 Ma (2 s.d.; $n = 12$; MSWD = 0.63) for EIN1607 and 1563 ± 15 Ma (2 s.d.; $n = 22$; MSWD = 0.30) for EIN1611, which are consistent with previously published U–Pb dates for metamorphic zircon in similar lithologies (1553 ± 3 Ma $^{207}Pb/^{206}Pb$ weighted mean age)[46]. Zircon from amphibolites EIN1607 and EIN1611 yields median $\delta^{18}O$ values of 1.5 ± 0.3‰ (2 s; $n = 9$) and 2.9 ± 0.6‰ (2 s; $n = 7$), respectively (Fig. 2A). Garnet from EIN1607 and EIN1611 has median $\delta^{18}O$ values of 1.9 ± 0.5‰ (2 s; $n = 24$) and 2.2 ± 0.7‰ (2 s; $n = 31$), respectively. While the studied amphibolites are metamorphosed basalts or dolerites initially produced through mantle partial melting[45], our data reveal that their oxygen isotopic composition is not representative of such a source, with $\delta^{18}O$ values more than 2‰ lower than those of mantle zircon (5.3 ± 0.6‰)[54]. A light oxygen isotope composition in mafic rocks is characteristic of high-temperature hydrothermal alteration by seawater or meteoric water[31].

Zircon from tonalite yields $^{207}Pb/^{206}Pb$ weighted mean ages of 1554 ± 13 Ma (2 s.d.; $n = 11$; MSWD = 0.33) for sample ES07aG, 1558 ± 19 Ma (2 s.d.; $n = 5$; MSWD = 0.5) for ES07aV, and 1567 ± 16 Ma (2 s.d.; $n = 7$; MSWD = 1.6) for ES31, consistent with the established timing of anatexis in the eastern inlier. Zircon portions dated at 1565–1550 Ma have homogeneous $\delta^{18}O$ values with medians of 6.1 ± 0.2‰ (2 s; $n = 5$) for ES07aG, 5.8 ± 0.4‰ (2 s; $n = 5$) for ES07aV, and 5.8 ± 1.3‰ (2 s; $n = 8$) for ES31 (Fig. 2A). These mantle to near-mantle values contrast sharply with the low $\delta^{18}O$ of the amphibolites from which the tonalite veins were derived. Thus, the partial melting of amphibolite producing tonalite in the eastern Georgetown Inlier was accompanied by a critical oxygen isotopic shift from ~1–3‰ to ~6‰ $\delta^{18}O$ values (Fig. 2A).

Sediment-derived (S-type) granites. Garnet–biotite-bearing granitic vein ES19 (eastern inlier) and rhyolite RR72 (western inlier) yield zircon median $\delta^{18}O$ values of 8.2 ± 0.4‰ (2 s; $n = 24$) and 8.3 ± 0.55‰ (2 s; $n = 23$), respectively. A sub-volcanic garnet–biotite granite RR71 (western inlier) shows bimodal O signatures with median $\delta^{18}O$ values of 8.7 ± 0.6‰ (2 s; $n = 27$) and 6.2 ± 0.3‰ (2 s; $n = 19$). Biotite–muscovite granites RR75 and RR77 (central domain) have zircon median $\delta^{18}O$ values of 6.1 ± 0.7‰ (2 s; $n = 23$) and 6.1 ± 0.1‰ (2 s; $n = 2$), respectively (Fig. 2A). Therefore, sediment-derived magmatic rocks thought to have been generated through water-flux melting at moderate temperatures (c.

750 °C) have distinctly lighter zircon oxygen isotope compositions (~6‰) than those derived from closed-system dehydration melting (8.3‰) at temperatures above 800 °C. The subvolcanic intrusion may show a hybrid O isotope signature reflecting interaction between the host metasedimentary source and hydrous magmas during ascent to upper crustal levels.

Metasomatic rocks. Metasomatic rocks in the eastern domain are exposed as a ~15-m-long, up-to-2-m-thick lens of garnetite (Fig. 1D) composed of cm-sized garnet, minor clinopyroxene and interstitial quartz and epidotised plagioclase (Fig. 1E), along with accessories such as zircon, titanite and allanite. The garnetite (ES34 and ES36) formed through partial melting of amphibolites and was brecciated during the intrusion of fracture-filling tonalite (EIN1702). The garnetite is composed of a garnet–clinopyroxene core (ES34) with mostly monomineralic (only garnet or clinopyroxene) or bimineralic (garnet and clinopyroxene) volumes, whereas the rim (ES36) is characterised by 0.5–4-cm-large hornblende and hornblenditic portions ± garnet, together with interstitial quartz and epidote (former plagioclase). Quartz and plagioclase exhibit interstitial textures between garnet and clinopyroxene crystals, supporting the coexistence of the garnet–clinopyroxene assemblage with the associated tonalitic melts.

A precise Lu–Hf, garnet–clinopyroxene isochron date of 1542.8 ± 2.2 Ma is obtained for garnetite sample ES36, which agrees with the 1565–1540 Ma age of the studied high-grade metamorphic and magmatic episode in the Georgetown Inlier[46,50].

Only a few prismatic zircon grains with concentric zoning, typical of a magmatic origin, were obtained from the garnetite sample, and these were generally low in U content (2–18 ppm), preventing precise age determination. Other grains yielded strongly inherited dates or discordant or reset isotopic ratios. Only two spots for ES34 yield relatively reliable individual $^{207}Pb/^{206}Pb$ dates at 1471 ± 24 Ma (2 s.d.) and 1507 ± 20 Ma (2 s.d.). Sample ES36 also yield Th/U ratios of <0.05 and a $^{207}Pb/^{206}Pb$ weighted mean age of 1543 ± 7 Ma (2 s.d.; $n = 4$; MSWD = 1.5), consistent with the obtained Lu–Hf date. Garnetite samples ES36 and ES34 have consistent zircon median $\delta^{18}O$ values of 6.3 ± 0.8‰ (2 s; $n = 13$) and 5.9 ± 0.5‰ (2 s; $n = 4$), respectively. In addition, garnet has median $\delta^{18}O$ values of 5.2 ± 0.3‰ (2 s; $n = 26$) for garnetite ES34 and 4.9 ± 0.7‰ (2 s; $n = 30$) for the associated tonalite EIN1701. The evident deviation between zircon and garnet $\delta^{18}O$ values is more pronounced for ES34 ($\Delta^{18}O = \delta^{18}O_{zircon} - \delta^{18}O_{garnet} = +1.0 ± 0.5‰$) than for amphibolite EIN1611 ($\Delta^{18}O = +0.7 ± 0.7‰$). This is consistent with a higher grossular content in ES34 garnet than in EIN1611 garnet, and with increasing zircon–garnet oxygen isotope fractionation from almandine to grossular garnet[55].

Discussion

Isotopic shifts during partial melting

Fluid-rock interaction can be traced by evaluating variations in the $^{18}O/^{16}O$ ratio of minerals within well spatially and temporally constrained association of source and melt products, making oxygen isotope compositions of resilient minerals such as zircon and garnet a powerful tool to reveal the magma and fluid source in which they crystallised[54,56,57]. Seawater typically has $\delta^{18}O$ values around 0‰ ($\delta^{18}O$ is the per-mil deviation of the $^{18}O/^{16}O$ ratio from the Vienna Standard Mean Ocean Water; VSMOW), whereas mantle-derived materials, such as mid-ocean ridge basalt, exhibit relatively homogeneous O isotope compositions ($\delta^{18}O = 5.3 ± 0.6‰$; 2 SD)[31,32]. Supra-mantle (heavy) $\delta^{18}O$ values (up to 30‰) typically indicate the incorporation of supracrustal materials that have experienced low-temperature hydrothermal alteration[31]. In contrast, sub-mantle (light) $\delta^{18}O$ values are generated by interaction with high-temperature (>300 °C) hydrothermal fluids that are produced by the interaction with seawater ($\delta^{18}O \approx 0‰$) and/or meteoric water ($\delta^{18}O_{meteoric\ water} << 0‰$, possibly down to −55‰)[58,59].

While purely sediment-derived granite commonly records $\delta^{18}O$ values ranging between 10 and 20‰[32,60,61], the studied volcanic and granitic rocks

Fig. 2 | O-isotope compositions for the investigated samples and worldwide dataset. A Variations in oxygen isotope compositions of zircon (δ¹⁸O(zircon)) from amphibolite, tonalite, garnetite and S-type granites from the Proterozoic Georgetown Inlier. **B** Compilation of δ¹⁸O(zircon) versus U–Pb age (Ma)[35,36,48,59,78] compared to the investigated samples and the range of average mantle zircon value[15].
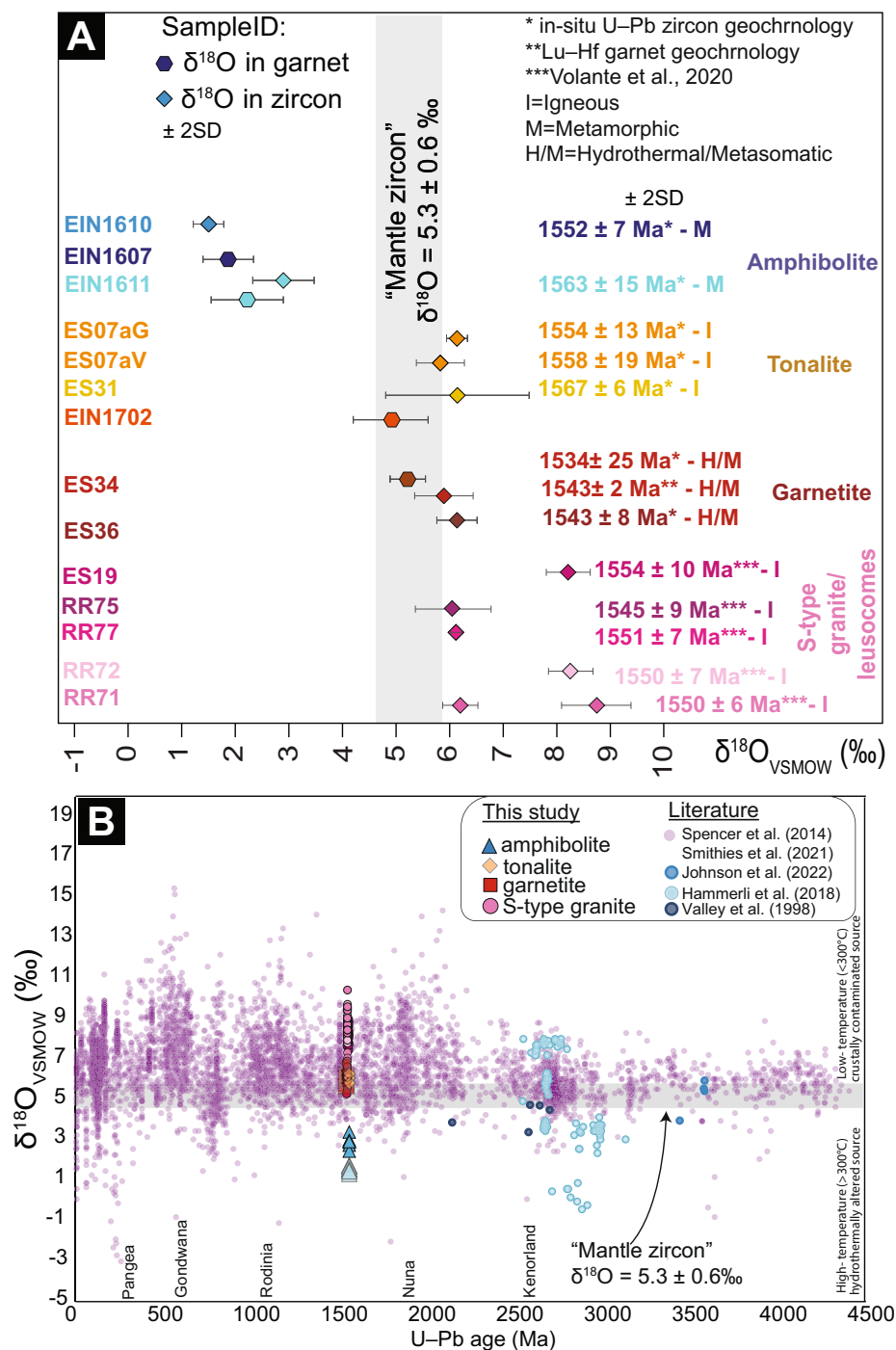
yield relatively lighter oxygen isotope compositions, with the colder, hydrous S-type granites exhibiting even lower values than the hotter anhydrous equivalents (6‰ versus 8‰ median δ¹⁸O values, respectively). This isotopic deviation from the source rock to its melting product supports the previously suggested contribution of extraneous materials (rock or fluid), with the latter being a mantle-derived source that mixed with heavier sediment-derived material in greater proportions in low-temperature, wet granites compared to the higher-temperature magmas[62–64]. The bimodal distribution of δ¹⁸O values between the low-temperature hydrous and the higher-temperature anhydrous granites from the Georgetown Inlier is likely structurally linked by water-fluxed melting along the crustal-scale detachment zone, juxtaposing the upper crustal domain to the mid-to-lower-crustal domain (Supplementary Fig. S1). The low-temperature hydrous granites formed at mid-crustal levels within a detachment zone, which acted

as a network facilitating the migration of mantle-derived fluids through the mid-crust, thereby triggering pervasive sediment-derived melting. In contrast, hotter, drier magmas ascended from the lower crust in the eastern domain to upper crustal levels, where their interaction with mantle-derived fluids was likely limited, resulting in predominantly median δ¹⁸O values of 8‰ (Fig. 2A).

Extensive field observations indicate that the tonalites exposed in the eastern Georgetown Inlier originated from partial melting of local amphibolite (Fig. 1A, B). The significant δ¹⁸O shift between the tonalite veins (6‰) and their source (1–3‰) supports the requirement for an external source material that caused the variation in δ¹⁸O values between the source and the melt product, which would otherwise have had a homogeneous oxygen isotope composition record. Thus, previously proposed water-fluxed melting as dominant mechanism for partial melting of the local

amphibolite is here confirmed. Additionally, the consistent $\delta^{18}O$ values (6‰) in the tonalite samples from both the northern (with incipient melting of the amphibolite) and southern (with extensive melting of the source rock) areas of the eastern domain suggests that the amphibolite does not contain regions with highly variable isotopic compositions. Metamorphic temperatures recorded by the amphibolite do not exceed 750–800 °C[15], yet partial melting is widespread in the mafic lower crust (i.e. 9 kbar) of the inlier[48,49], indicating pervasive fluid flow through the mafic lower crust might be required. Conversely, extensive migmatization in the paragneiss shows evidence of both fluid-absent and fluid-present melting, suggesting that this metasedimentary package was less exposed to mantle-derived fluids and that fluid flow was confined to discrete pathways. This confinement likely resulted in leucosomes with higher $\delta^{18}O$ values (8‰) compared to the amphibolitic lower crust (1–3‰) and the associated tonalitic melt (6‰).

We propose that, like the S-type granites, the $\delta^{18}O$ shift from amphibolite to tonalite reflects the substantial influence of external fluid material that differ isotopically from the source rock. The oxygen isotope data for the tonalites align with petrographic observations and previous thermodynamic modelling, indicating that amphibolite partial melting occurred at relatively low temperatures (750–800 °C), driven by fluid flux.

While both paragneiss and amphibolitic partial melting in the Georgetown Inlier required external fluid addition, direct evidence for intensive fluid circulation through the lower crust is provided by the garnetite residue in the eastern domain. The oxygen isotope composition of the garnetite matches that of the low-temperature granites and tonalite, suggesting that the formation of the garnetite, like the partial melting of metasedimentary rocks and amphibolite, involved isotopically similar fluids, with an overall median $\delta^{18}O$ value of 6‰.

Low $\delta^{18}O$ amphibolite

Zircon grains from ~1555 Ma amphibolite samples exhibit low $\delta^{18}O$ values, ranging from 1.2 to 3.0‰ (Fig. 2A). This contrasts sharply with most published magmatic zircon $\delta^{18}O$ data for amphibolite, which typically range from 5 to 15‰[65] (Fig. 2B). These higher values generally imply zircon sourced from mantle-derived melts (i.e. $\delta^{18}O = 5.3 \pm 0.6$‰)[32] that mixed with varying amounts of crustal contaminants, such as marine sediments with $\delta^{18}O$ values of 10–30[31]. In contrast, sub-mantle $\delta^{18}O$ values in mafic rocks have been linked to high-temperature interactions with seawater ($\delta^{18}O = 0$‰)[66] and/or meteoric water ($\delta^{18}O$ as low as −55‰)[30,31,67,68] during or shortly after basaltic magma emplacement[14].

One interpretation is that the basaltic protolith interacted with high-temperature hydrothermal fluids shortly after its emplacement around 1665 Ma, thereby acquiring a low whole-rock $\delta^{18}O$ value. This signature was later incorporated into the zircon and garnet during metamorphism and partial melting at 1555 Ma. However, this scenario is complicated by the amphibolites' characteristics, such as plagioclase breakdown and high degrees of melting, despite rather moderate peak temperatures (750 °C). These features suggest that partial melting occurred through fluid flux under open-system conditions. Notably, all investigated tonalites, sediment-derived granites, and the garnetite share a consistent $\delta^{18}O$ value of ~6‰, indicating that the amphibolites were not exposed to fluids of different composition than those affecting the other rock types. Hence, an alternative explanation is that the amphibolites' $\delta^{18}O$ values increased due to the influx of mantle-derived fluids (~6‰ $\delta^{18}O$) around 1555 Ma, implying the basaltic protolith may have experienced even lower $\delta^{18}O$ values during high-temperature hydrothermal alteration. Another possibility is that the residual garnetite represents a discrete lens with sharp contacts with the surrounding paragneiss, where tonalitic veins and dykes often intrude the host migmatites. This would explain why the amphibolites have retained their original $\delta^{18}O$ signature, while the garnetite exhibits a mantle-like $\delta^{18}O$ value.

Composition and abundance of the fluxed fluid

Using a Monte Carlo simulation approach, we explore various fluid–rock interaction scenarios that could explain the oxygen isotope signatures documented in this study. The simulation considers different proportions of

mantle-derived melt, crustal material, and seawater and/or meteoric water with varying $\delta^{18}O$ values (Supplementary Data Table S6).

First, we examine the deviation of the amphibolite samples ($\delta^{18}O = 1$–3‰) from the expected mantle value (5.3 ± 0.6‰). This significant decrease in $\delta^{18}O$ indicates high-temperature interactions with ^{18}O-depleted hydrothermal fluids, likely seawater ($\delta^{18}O \approx 0$‰) or meteoric water ($\delta^{18}O = -10^{+10}_{-20}$ ‰), or both. We calculate water–rock mixing scenarios using a published water-to-rock proportion range of 0.01–2, with a mode of 0.18[58]. This range aligns with present-day ratios and represents the threshold at which additional fluid cannot further alter a rock. Although Precambrian water–rock interaction processes are not fully understood, this broad range is unlikely to have dramatically changed since the Archaean, with secular variations likely affecting only the mode. Modelling shows that the $\delta^{18}O$ values of the amphibolite samples ($\delta^{18}O = 2.0^{+1.0}_{-0.6}$‰) cannot be reproduced through interaction with seawater (Fig. 3A), which yields normally-distributed $\delta^{18}O$ values of 4.3 ± 0.9‰ (with 95% confidence intervals). In contrast, a positively skewed $\delta^{18}O$ distribution of $1.9^{+2.6}_{-4.9}$ ‰, overlapping with the measured compositions, is obtained from mixing with meteoric water (Fig. 3B). The wide range of calculated $\delta^{18}O$ values reflects the diverse compositions of meteoric water considered in the calculation. The oxygen isotope composition of meteoric water is significantly influenced by latitude and elevation[69], which are not well constrained for the Georgetown Inlier at 1665 Ma. Despite uncertainty regarding the amount of fluid involved, it can be concluded that the studied amphibolites acquired their low-$\delta^{18}O$ signature through alteration of their basaltic protolith by meteoric water following the emplacement around 1665 Ma.

The second fluid–rock interaction scenario involves the formation of S-type granitic magma with $\delta^{18}O$ values distinctly lower than those typically expected for paragneiss and micaschist, which range from 10‰ to 20‰[32]. Granite samples show a bimodal distribution of zircon $\delta^{18}O$, with medians of ~6‰ and ~8‰ for the central and eastern domains, respectively (Fig. 3C, D). Pure crustal granite derived solely from metasedimentary sources is relatively rare globally; rather, regional and global databases reveal a chemical and isotopic continuum between purely sedimentary and purely mantle-derived sources[63,64,70,71]. The two isotopically distinct igneous zircon populations obtained from an individual sample (sub-volcanic granite RR71) suggest mixing between two chemically distinct sources (i.e., those represented by the eastern and central domains), rather than assimilation of lower-$\delta^{18}O$ country rock during magma ascent. Consequently, we modelled the interaction between a sedimentary protolith and a mantle-like fluid to determine the proportions of crustal contaminants necessary to generate the sediment-derived granitic magma from the Georgetown Inlier (Fig. 3C, D). Since the isotopic composition of the sedimentary protolith is unknown, a theoretical metasedimentary source is proposed with $\delta^{18}O$ values ranging from 10‰ to 30‰ $\delta^{18}O$ and a mode at 15‰, consistent with commonly accepted values for siliciclastic rocks[31]. We use different distributions of crustal assimilant-to-parent rock proportions of 0.001–0.15 (mode = 0.1) and 0.001–0.6 (mode = 0.4) to effectively model the central and eastern domains, respectively. These crustal assimilant-to-parent rock proportions yields good fits for both the central and eastern domains, with the modelled modes within 0.1 ‰ of the measured data (Fig. 3C, D). The modelling results for the sediment-derived melts indicate that the leucosomes from the eastern domain require about four times more crustal assimilants to reach $\delta^{18}O$ values of 8‰ compared to the granites in the central domain.

Finally, an external fluid was involved during flux melting of amphibolite to produce tonalitic melts. Previous petrological and modelling constraints[4,15] are here confirmed by the large isotopic shift from 1 to 3‰ to 6‰ that occurred during anatexis. Mixing melts derived from the amphibolite (i.e. samples EIN1607 and 1611, $2.0^{+1.0}_{-0.6}$‰) with typical depleted mantle (5.3 ± 0.6‰), can generate the tonalitic melt mode (5.0 ± 0.5‰) but fail to properly capture its negatively skewed distribution of $5.5^{+1.5}_{-0.8}$‰ (Fig. 3E). Thus, to obtain a negatively skewed $\delta^{18}O$ distribution for the tonalites, a component isotopically heavier than mantle (5.3 ± 0.6‰) is required, most likely from a sedimentary source (Fig. 3E). We consider three-component mixing of amphibolite ($2.0^{+1.0}_{-0.6}$‰), mantle-like material
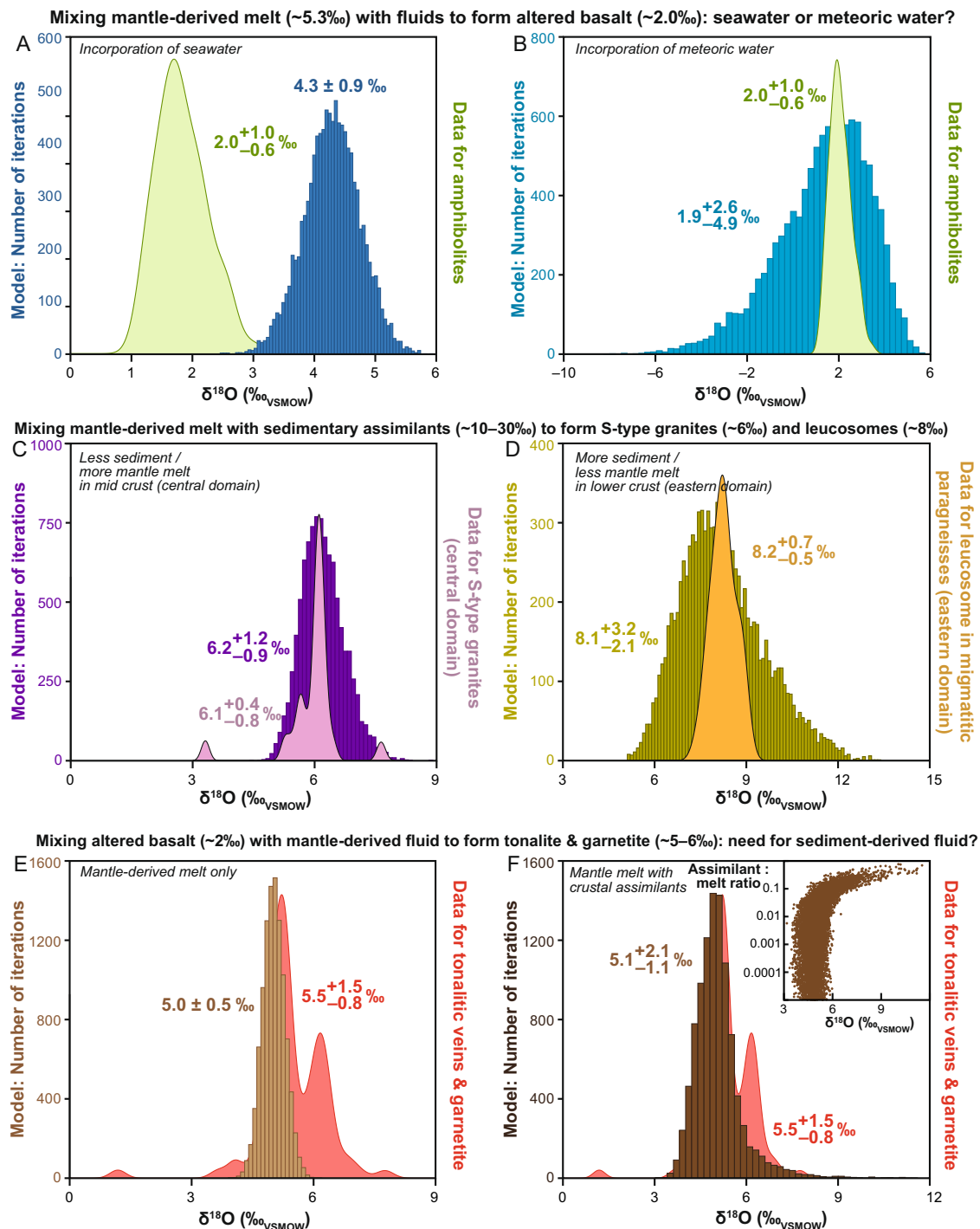
Fig. 3 | Monte Carlo δ18O mixture models of mantle-derived melts, crustal assimilants, seawater and meteoric water. Histograms of Monte Carlo simulations of various O isotopic reservoirs compared to probability density plots of zircon and garnet O isotopic data. **A** Mixture of mantle-derived melt with seawater is unable to reproduce the amphibolitic gneiss. **B** Mixture of mantle-derived melt with meteoric water overlaps with amphibolitic gneiss albeit with too large a spread. **C** Mixture of mantle-derived melt with sedimentary assimilants to form S-type granites from the central domain. **D** Mixture of mantle-derived melt with sedimentary assimilants to form hybrid S-type granites from the western domain and leucosomes from the eastern domain. **E** Mixture of mantle-derived melt with basaltic protolith is unable to yield supra-mantle tonalite and garnetites O isotopic data. **F** As in (**E**) but adding in small proportions of isotopically heavy crustal (sediment-derived) contaminants to also produce supra-mantle tonalite and garnetite. Inset: cross-plot of assimilant-to-mantle ratio vs. δ18O.

$(5.3 \pm 0.6‰)$ and a theoretical siliciclastic source $(15^{+15}_{-5}‰)$. A distribution of $(5.5^{+1.5}_{-0.8}‰)$ can be modelled with a negatively skewed distribution $(-5.1^{+2.1}_{-1.1}‰)$ that approximates the measured data. These results indicate that, in most cases, assimilation of sedimentary material is rare (<1% assimilant, 0.01:1 ratio of assimilant to melt) to yield δ18O of ~5.5‰, but occasionally, up to 20% assimilant (0.2:1 ratio of assimilant to melt) is

required to reach δ18O as high as $7.8 \pm 0.4‰$ observed in the tonalite (Fig. 3F).

In summary, statistical modelling shows that sediment- and amphibolite-derived magmatic rocks in the Georgetown Inlier were generated through the ingress of abundant external fluids, predominantly sourced from a mantle-like reservoir. The involvement of sedimentary

Fig. 4 | Tectonic sketch of the Georgetown Inlier during post-collisional extension at c. 1550 Ma. Rollback of the Laurentian lower plate drove progressive opening of the mantle wedge window, facilitating fluid circulation that partially melted the metasomatized mantle. Mafic underplating formed at the base of the lower crust, which exsolved those mantle-derived fluids carried while crystallising triggering fluid-fluxed melting of the amphibolite and generation of TTG magmas and associated metasomatic restitic rocks (modified after[44]).
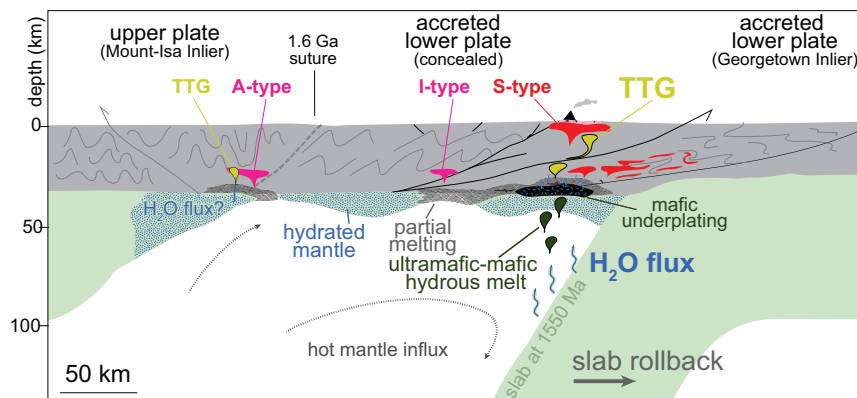
material in the isotopic signatures of amphibolite-derived magmas may be related to direct assimilation of metasedimentary material or interaction with fluids derived through dehydration melting of fertile sedimentary rocks.

Source(s) of the melt-triggering fluid

Our study provides evidence for the circulation of mantle-like fluids triggering melt in the lower crust of a Proterozoic orogenic system. Mantle-like fluid sources have been discussed for other regions worldwide[24,25,36,37,42,63,72,73], generally falling in two categories: (i) hydrated lithospheric mantle and (ii) hydrous mafic underplates accumulated during active subduction. Summarising the tectonic evolution of the Georgetown Inlier helps identifying the reservoir involved in this study.

Recent research has clarified the tectonic and metamorphic evolution of the Georgetown Inlier. These studies indicate that the inlier was part of a Laurentia-derived continental terrane[74] that accreted to the Mount-Isa Inlier —the eastern margin of the North Australian Craton (NAC)—between 1610 and 1590 Ma during a 'soft' continental collision[47,75]. The absence of subduction-related magmatism, combined with extensive deformation resulting in a regional-scale, asymmetrical bivergent thrust wedge, suggests a hot continental collision (i.e. with elevated metamorphic thermobaric ratios), which is characteristic of Proterozoic orogens[76]. The exact location of the concealed 1600 Ma suture remains debated[44,47,52,77] but contrasting metamorphic histories at 1610–1590 Ma indicate that the Georgetown Inlier belonged to the lower plate, while the Mount-Isa Inlier was part of the upper plate[44,74].

Following the continental collision around 1600 Ma, the Georgetown Inlier was partially exhumed along a shallow, west-dipping crustal-scale detachment zone and subsequently experienced heating and magmatism at 1565–1540 Ma, likely in an extensional regime[49,51] related to protracted slab roll-back[44,50] or sub-continental lithosphere delamination[75] (Fig. 4). Protracted slab-roll back drove progressive opening of the mantle wedge from west to east, which triggered partial incorporation of lower-plate crustal material into the upper plate during repeated extensional-contractional phases[78]. Post-collisional igneous activity shows a regional chemical pattern of west-to-east migration of hydrous felsic magmatism, starting from 1570 Ma in the easternmost NAC and reaching the Georgetown Inlier by 1565–1545 Ma. Around 1545 Ma I-type granites were emplaced between the Georgetown and the Mount-Isa inliers, whereas between 1540 to 1490 Ma, hot and dry (i.e. A-type) granitic intrusions occurred in the eastern NAC. During this extensional stage, felsic magmatism shifted from low-temperature, hydrous conditions to high-temperature, dehydration-driven crustal melting, likely due to lithospheric thinning. Upwelling of the asthenospheric mantle above a retreating or delaminating lithospheric slab likely provided significant heat and fluids to the base of the partially exhumed Georgetown Inlier, which, in this scenario, became part of the upper plate material during the development of the extensional detachment zone and

hydrous magma generation. However, this scenario would likely produce high-Mg andesite to dacitic type of magmas in the above upper plate at 1565–1540 Ma, which are not observed in the study area. An alternative scenario is that water from a down-going slab migrated to the surface, producing hydrous mafic magmas by partial melting of the metasomatized mantle during opening of the wedge. During this ascent, mafic magmas fractionated, cooled and exsolved water, triggering flux melting of the lower crust. Although mafic magmatism from this period is generally absent, Hf model ages between 1585 and 1545 Ma have been found in modern detrital grains of Siluro-Devonian igneous zircons in the region, suggesting that isotopically primitive mafic rocks formed during this time[50,79]. It is inferred that this mafic reservoir formed during mantle-crust decoupling, inducing asthenospheric inflow beneath the Georgetown Inlier, providing a potential source of mantle-like fluids that triggered fluid-flux partial melting of the crust. An alternative scenario might involve those regional deep crustal fluids acquiring a 'mantle-like' signature by interacting with local amphibolitic (with light $\delta^{18}O$) and metasedimentary (with heavier $\delta^{18}O$) crustal rocks, averaging to an oxygen composition of 6‰. However, this interpretation would likely generate heterogeneous fluid compositions across different lithologies, whereas the consistent 5–6‰ $\delta^{18}O$ signatures observed across the tonalite, garnetite residue, and S-type granites suggest that the influx of a fluid with a similar composition produced these isotopic signatures at 1555 Ma. Furthermore, the tectonic setting and the general agreement on the presence of mafic underplating in NE Australia during the Mesoproterozoic[80,81] support the interpretation that the fluids triggering partial melting were indeed exsolved from mantle-derived mafic underplating (below referred to as mantle-derived fluids). Regardless of the tectonic model for the Proterozoic orogenic system, our findings show unequivocally low $\delta^{18}O$ values in zircon and garnet from an amphibolite source, as well as mantle-like values in associated tonalite, garnetite and S-type granites. These results strongly suggest the ingress of external fluids during anatexis and the significant role of mantle-derived fluid-flux melting in forming new continental crust within a convergent setting, highlighting the sources and pathways of water during crust formation processes.

Secular oxygen isotope changes of new and recycled continental crust

Water-flux melting has been reported within various tectonic, crustal settings and its manifestation can be observed from localised to regional scales[1,6,9,21]. The availability of fluids greatly influences the volume of melt produced, sparking interest in identifying their sources[24,32,37]. Global compilations show that nearly all zircon $\delta^{18}O$ data from Precambrian crustal rocks fall within a 5–8‰ range[62,65,72] (Fig. 2B). However, oxygen isotope data for mafic rocks are scarce. Valley et al.[38] first recorded Precambrian zircon from mafic-ultramafic rocks with the lowest $\delta^{18}O$ values—ranging from 3.4 to 4.7‰—compared to mantle zircon (Fig. 2B). These low $\delta^{18}O$ signatures were interpreted as indicative of subduction-related processes, where late

Fig. 5 | Synoptic diagrams showing plausible end-member tectonic scenarios for water-present melting generating TTG crust during the Pre-cambrian. A A warm Precambrian subduction zone shows the opening of the mantle wedge during slab breakoff inducing heat, fluid circulation, mantle metasomatism and fluid flux of the mafic lower crust to produce TTG plutons. **B** TTG generation by fluid-fluxed melting of mafic crust in an intraplate setting where water is introduced in the mantle during vertical sinking of hydrated mafic–ultramafic crust.
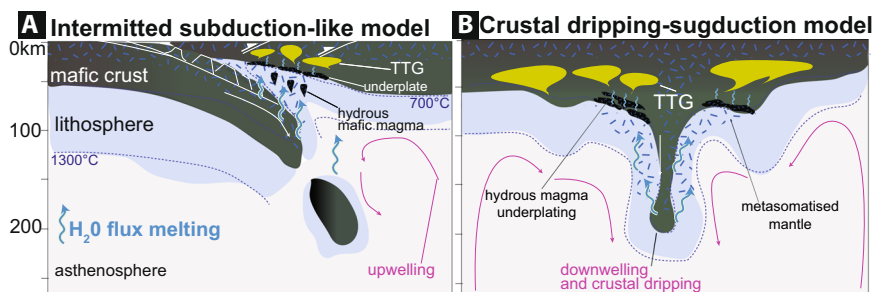
Archaean oceanic crust exchanged oxygen with heated seawater before underplating and subsequent metasomatism of the mantle wedge. Others have interpreted extremely low $\delta^{18}O$ values in zircon from mafic granulites from the Yilgarn Craton as evidence for high-temperature hydrothermal interactions between the protoliths and shallow crustal materials, as well as ^{18}O-depleted meteoric fluids, resembling conditions in the Yellowstone caldera[42]. In the Pilbara Craton, low $\delta^{18}O$ values (3.8–4.7‰) relative to mantle zircon have been attributed to: (i) intense and prolonged hydrothermal circulation of fluids through a highly fractured mafic-ultramafic crust-shell after giant impacts in the early Earth[25]; (ii) partial melting of a hydrous mafic source enriched by primordial mantle-derived fluids[24]; or (iii) the existence of rock-fluid interactions involving meteoric water dating back to c.4.0 Ga[37].

In this study, statistical mass balance calculations of fluid–rock interactions explain the oxygen isotope shifts during partial melting as triggered by mantle-like fluids. Hydrous fluids rising from the slab as the mantle wedge opens produce hydrous basaltic magmas. These hydrous magmas then underplate the lower crust and exsolve their water as they crystallise. This water triggers low-temperature partial melting of the overlying crust. Water-flux melting plays a key role in buffering the oxygen isotope signature of the surrounding rocks, provided the influx of mantle fluid is maintained as successive mafic underplates reach water saturation and release a fluid phase[1]. Localised high-fluid activity can promote rapid and extensive partial melting of the mafic lower crust, producing significant amounts of felsic melt with a mantle-like oxygen isotope signature, contributing to a slightly heavier $\delta^{18}O$ signature in the low $\delta^{18}O$ amphibolite source.

By contrast, generation of S-type granites at mid to upper amphibolite-facies reflects a mantle-like oxygen isotope signature that is responsible for a lighter $\delta^{18}O$ signature (6‰) than expected from melted metasedimentary protoliths. Additionally, compared to the higher $\delta^{18}O$ values (8‰) of the higher-temperature, S-type volcanic and subvolcanic rocks of the upper crustal, western Georgetown province, the low $\delta^{18}O$ values recorded by S-type granites in the mid-crustal central domain confirm the need for external water to produce voluminous crustally derived (S-type) magmas[4] (Fig. 3C). Our findings highlight the critical role of mantle-derived fluids in driving crustal anatexis at lower to mid-crustal levels, thereby influencing geochemical evolution of the continental crust within convergent settings.

Water-flux melting as key ingredient for crustal growth through Earth history

In the past decades, water availability has been more extensively demonstrated to play a crucial role in lowering the solidus temperature to produce partial melting of basaltic rocks and abundant felsic melt together with its influence on the composition of the restite and the produced melt[9,15,26]. Considering that most of the felsic crust was produced by the end of the Archaean, water must have played, together with heat, a key role in the formation of the nuclei in the early Earth. Several studies provide evidence indicating that water is likely a key ingredient in the production of felsic crust, and different water sources were proposed[1,5,6,9,10,16,21,24,25].

Whereas for well-constrained Proterozoic (Fig. 5) and Phanerozoic convergent settings water-flux melting has been commonly related to fluids

deriving from a subducting slab[11,12,44] or from water-rich crustal material[9,16], the Archaean was most likely dominated by vertical-tectonics[82,83] raising questions such as (i) was water-flux melting an important mechanism for crust production and if so (ii) what was the source of the fluxing water. Combined isotope geochemistry[22] and analytical modelling[23], along with thermodynamic modelling[15,26,29,84], studies have demonstrated that water-flux melting was an important physicochemical mechanism in the early Earth, if not the most dominant one. During the first two billion years of Earth's history, the source of the water that fluxes the lower crust to generate sodic magmas has been attributed to different reservoirs. A few studies used geochemical and petrological data to demonstrate that a great amount of water was accommodated as crystal-bound OH− in ferromagnesian hydrous minerals such as chlorite, serpentine and amphibole of high-MgO mafic-ultramafic rocks[84–87]. In this scenario, Archaean komatiites were demonstrated to be able to carry about four times more water than high-MgO mafic-ultramafic rocks subsequently released at low temperatures, 700–750 °C[87]. Thus, high-MgO mafic-ultramafic rocks in the Hadean and Archaean may have been an important source of water in the deep crust and/or lithospheric mantle. Other studies have used bulk-rock geochemistry and oxygen isotope compositions of zircon to argue that primordial water was already present in sufficient amounts in the ancient mafic lithosphere to produce primitive sodic felsic crust[24].

Due to poor preservation of the ancient rock record, the source of the fluids triggering partial melting of the crust is commonly investigated in the produced sodic melt. Mantle-like or slightly heavier $\delta^{18}O$ signatures of zircon for most Archaean and Hadean TTGs have been interpreted to reflect the interaction of hydrous basaltic source rocks with supracrustal material and alteration by low-temperature hydrothermal fluids[25]. On the other hand, mantle-like sensu-stricto signatures of zircon grains from MgO-rich primitive TTGs have been proposed to reflect hydration of basaltic source by primordial mantle-derived water at lower crustal conditions or in the lithospheric mantle[24]. The latter scenario suggests that the early Earth's mafic crust was already carrying enough water to produce voluminous amounts of primitive granitoids to form sodic continental nuclei[24,88,89]. By contrast, isotopically light $\delta^{18}O$ values of ancient detrital or magmatic zircon require the interaction of shallow crustal magmatic systems with meteoric water, which have led different authors to suggest that the emergence of the first continents and their interaction with fresh water marked the beginning of the hydrological cycle only 500 million years after the formation of the Earth[37,90].

The global ocean, covering the erupting MgO-rich basaltic and komatiitic lavas in the early Earth, allowed for constant hydration and alteration of the mafic and ultramafic crust. Tectonic regimes such as sag-duction (Fig. 5) include a valuable way to bring fluids at deeper crustal levels and release them at relatively low temperatures of 700–750 °C[84]. Alternatively, or in combination with the first scenario, hydrous mafic-ultramafic material building the lithospheric mantle and the lower crust was, at least locally, continuously water-saturated such that when those temperatures were locally reached water would be released to form hydrous mafic melts that would raise and form mafic underplates at the lower crust where they would start to exsolve water while crystallising. The well-exposed and

structurally well-constrained case study from the Proterozoic orogen in NE Queensland should, therefore, may serve as example for the Archaean community to further investigate ancient terranes where preserved association of rocks including potential source rocks, produced melts and restitic rocks can be used to trace the origin of water in the early Earth and its implication in the formation and alteration of ancient cratons.

Methods

Sample preparation

Zircon grains were extracted from each sample via standard procedures, mounted in epoxy, and polished.

Garnet was separated and prepared in different ways depending on the samples. For those containing centimetre-large crystals (EIN1702 and ES34), portions of rock were drilled out, trimmed, mounted in epoxy, and polished. For other samples, entire garnet grains were extracted using crushing, fragmenting, hand-panning, and hand-picking (EIN1607, EIN1611) and then mounted in epoxy, ground down to their approximate geometric centre, and polished. In addition, an EIN1607 polished thin section was drilled to extract a garnet grain.

Zircon analytical targets were identified using secondary electron–, back-scattered electron– and cathodoluminescence imaging using a MIRA3 TESCAN scanning electron microscope at the John de Laeter Centre, Curtin University, Western Australia. Representative zircon zoning and analytical spots are shown in Supplementary Fig. S3.

Whole-rock geochemistry

Bulk-rock chemical data for the Georgetown mafic rocks were compiled from ref. 45 and two metamafic samples from ref. 15. Bulk-rock geochemical data for the Brandy Hot Granodiorite, Sawpit Granodiorite, and Talbot Creek Tonalite, members of the Forest Home Supersuite, are from the Geoscience Australia OZCHEM database (https://portal.ga.gov.au/persona/eftf). In addition, samples of the Forest Home Trondhjemite formerly analysed by Geoscience Australia were re-analysed by ref. 15 to obtain an expanded set of trace element data. Bulk-rock geochemistry data for the investigated S-type granites can be found in ref. 4. New sample investigated in this study include tonalitic leucosomes ES31, ES07aV, ES07aG and the metasomatic rock ES34. Samples were cast using a 66:34 flux with 4% lithium nitrate added to form a glass bead, which was then analysed for major elements via X-ray fluorescence (XRF) on oven dry (105°C) samples and for trace elements using laser ablation inductively-coupled plasma mass spectrometry (LA–ICP–MS). Loss-on-ignition values were determined using a robotic thermogravimetric analysis (TGA) system. A complete list of the bulk-rock chemical data for samples from the literature and this study is presented in Supplementary Data Table S2.

Zircon U–Pb dating via LA-ICP-MS

Zircon U–Pb measurements were collected from samples EIN1607, EIN1610, ES07aG, ES07aG, ES31, ES34, and ES36 were analysed for U–Th–Pb isotopes across two sessions at the GeoHistory Facility, JdLC, Curtin University. For both sessions, a RESOlution SE 193 nm ArF with a Lauren Technic S155 cell was used. The beam diameter was 30 μm, on-sample energy was 3.4–4.0 J cm^{-2} with a repetition rate of 5 Hz for 25 s of analysis time and ~45 s of background capture. All analyses were preceded by two cleaning pulses. The sample cell was flushed by ultrahigh purity He (0.32 L min^{-1}) and N2 (1.2 mL min^{-1}).

Zircon U-Pb isotope data were collected on an Agilent 8900 triple quadrupole mass spectrometer for all sessions with high-purity Ar as the carrier gas (flow rate 0.98 L min^{-1}). Analyses of ~20 unknowns were bracketed by analysis of a standard block containing the primary zircon reference materials GJ-1 (601.95 ± 0.40 Ma)[91,92] and OG1 (3465.4 ± 0.6 Ma)[93], which were used to monitor and correct for mass fractionation and instrumental drift. The standard block also contained the Phanerozoic to Archaean reference materials Plešovice (337.13 ± 0.37 Ma)[94], 91500 (1063.78 ± 0.65 Ma)[91,95] and Maniitsoq (3008.70 ± 0.72 Ma)[96]; all uncertainties at 2σ), which were used to monitor

data accuracy and precision. During the analytical sessions, when reduced against a matrix-matched reference material, Plešovice, 91,500 and Maniitsoq yielded statistically-reliable ($p > 0.05$) weighted mean ages of 338 ± 5 Ma to 340.3 ± 4.5 Ma, 1058 ± 19 Ma to 1060 ± 14, and 3010 ± 16 to 3010 ± 27 Ma (all uncertainties at 2 s.d.), respectively, all of which are within the published age (see Supplementary Data Table S3 for full reference material compilation).

U-Pb isotopic data were reduced in Iolite4[97]. Uncertainties on analyses of primary reference materials were propagated in quadrature to the unknowns and secondary zircon reference materials. For the unknowns, some analyses ablated across inadvertent inclusions; these inclusion-related signals were cropped from the integrations or, if too large or numerous, integrations were deleted; whilst the accuracy of the cropped analyses is maintained, the precision of the U-Pb data is significantly reduced due to the shorter integration times. No corrections were applied for common Pb because common Pb was below detection limits for almost all concordant analyses (f206). Zircon analyses are considered concordant where the error ellipses at 2σ generated by the $^{207}Pb/^{206}Pb$ and $^{206}Pb/^{238}U$ ratios overlap the inverse Concordia curve, excluding uncertainties on the decay constant. Age calculations and plots were made using Isoplot version 6.0[98]. All zircon dates are >1.5 Ga and are presented as $^{207}Pb/^{206}Pb$ ages for optimum precision[99]. All spot analyses are presented at 2σ, and weighted mean analyses are presented at 95% confidence. Full isotopic data for the reference materials and unknowns are given in Supplementary Data Table S3.

Electron microprobe analyser

Quantitative mineral-chemistry points and profiles analysis of major (Na, Si, Ti, Mn, K, Mg, Al, Fe and Ca) and trace elements (Cr and Y) were acquired using the Electron Microprobe Analyser (EPMA) JEOL 8200 electron microprobe equipped with five WDS spectrometers located at the Department of Earth Science, University of Milan. Major element compositions of garnet, pyroxene, amphibole, and feldspar (Supplementary Data Table S7) in samples EIN1611, EIN1702, and ES34 were determined using wavelength-dispersive spectrometry. The operational conditions were 15 kV and 20 nA specimen current. The analytical spot diameter was set at ~1 μm, keeping the same current conditions. Natural and synthetic standards were used for calibration. On- and off-peak counting times were 15 s and 20 s, and dead-time corrections were applied to all analyses.

Oxygen isotopes via SIMS (Cameca 1280)

In-situ oxygen isotope compositions ($^{18}O/^{16}O$) in zircon and garnet were measured using a SIMS (Cameca IMS-1280) at the Centre for Microscopy, Characterisation and Analysis (CMCA), University of Western Australia (UWA). Prior to SIMS analyses, mounts were carefully cleaned in ethanol and distilled water before coating with a 30 nm Au coating. For both O isotopes measurement in zircon and garnet, the sample surface was sputtered over a 10×10 μm area with a 10 kV, gaussian Cs$^+$ beam with intensity of 2.5 nA and a total impact energy of 20 keV. An electron gun was used to ensure charge compensation during the analyses. Secondary ions were admitted within a 110 μm entrance slit and focused on the centre of a 4000 μm field aperture (×130 magnification). Energy filtering was applied using a 40 eV band pass with a 5 eV gap toward the high-energy side. ^{16}O and ^{18}O were collected simultaneously in Faraday cup detectors fitted with 10^{10} Ω (L'2) and 10^{11} Ω (H1) resistors, respectively, and operating at a mass resolution of ~2430. The magnetic field was regulated using NMR control. Each analysis includes a pre-sputtering over a 15×15 μm area during 40 s, followed by the automatic centring of the secondary ions in the field aperture, contrast aperture and entrance slit. Each analysis then consists of 24 s cycles, which give an average internal precision of ~0.20–0.30 ‰ (2 SE). The analytical session was monitored in term of stability using at least two bracketing matrix-matched reference materials (see below) every 5–6 sample analyses. Bracketing of reference materials allowed for instrumental mass fractionation (IMF) and drift corrections. Corrected $^{18}O/^{16}O$ ratios are reported in δ^{18}O notation, in per mil variations relative to VSMOW.

For oxygen isotopes in zircon, instrumental mass fractionation was corrected using the zircon reference material 91500 (9.9 ± 0.3‰)[100], and accuracy was checked the secondary reference material OGC (5.88 ± 0.06‰)[101], which returned a $\delta^{18}O$ value of 5.68 ± 0.23‰. The spot-to-spot reproducibility on 91500 was ~0.30‰ (2 SD) during the analytical session. For oxygen isotopes in garnet, thin sections were cut with a precision saw and mounted in epoxy, together with pre-polished blocks containing a range of reference materials for O isotope measurements in garnet (as detailed below). The analytical session was monitored in terms of stability using at least two bracketing standards (UWG-2)[102], every 5 to 6 sample analyses. The spot-to-spot reproducibility on UWG-2 was ~0.24–0.30‰ (2 SD) during the analytical session. For garnet, the correction for instrumental mass fractionation has to account for the bias, or matrix effect, related to the difference in chemistry between the unknowns and the reference materials[56,103,104]. In absence of uvarovite and andradite components in garnet samples, the grossular component (X_{Gr}) creates the largest bias on oxygen isotope measurements by SIMS[56,103,104]. Therefore, five garnet reference materials, with different X_{Gr}, were analysed to model the matrix effect and correct the measurements of the unknowns. Oxygen isotope analyses in the samples were acquired next to the spot locations where EPMA measurements were performed for the matrix correction (Supplementary Data Table S7). The garnet reference materials used in this study were the same for the 2 mounts: 10691, 2B3, GRS-SE and UWG2 and ALM-GEM (in-house, X_{Gr} = 0.01, $d^{18}O$ = 6.79‰). For both mounts, the relationship between bias and X_{Gr} can be fit with a parabola, with a correlation coefficient (r^2) better than 0.97, returning a regression residual of ~0.3 per mil, in the range of the external reproducibility observed on UWG-2.

The uncertainty on single spot analyses reflects the residual observed on the calibration curve, which represent the average difference between the model and the measurements for the matrix effect calibration curve and the external reproducibility on UWG-2. Supplementary Data Table S4 presents the raw $^{18}O/^{16}O$ ratios and the corrected $\delta^{18}O$ values (quoted with respect to Vienna Standard Mean Ocean Water or VSMOW in per mil).

Garnet Lu–Hf geochronology

The timing of high-temperature metasomatism in sample ES34 was determined using Lu–Hf geochronology. Pure garnet and clinopyroxene were separated using crushing, sieving, hand-panning, and hand-picking. Garnet Lu–Hf chronology was carried out at the Pacific Center for Isotopic and Geochemical Research (PCIGR), University of British Columbia, Vancouver, following methods adopted from[105]. Target garnet aliquot weight was 50–80 mg, depending on the Hf concentration. Samples were mixed with a $^{176}Lu-^{180}Hf$ tracer solution (Lu/Hf ≈ 10) and digested through repeated addition of concentrated $HF–HNO3–HClO4$ and 6 N HCl, with intermittent evaporation to dryness. Matrix mineral aliquots free of garnet were mixed with a $^{176}Lu-^{180}Hf$ tracer solution with low Lu/Hf (~0.2) and dissolved using the same table-top dissolution technique or by adding $HF:HNO3$ and placing the samples in autoclaves at 180 °C for 5 days. Total procedural blanks were processed with every group of samples and held 10 pg of Hf or less, which enabled sample/blank Hf of 1000+ for garnet. Lutetium and hafnium were separated from their elemental matrix using cation-exchange REE–HFSE chromatography following a method adapted from ref. 106. Lutetium and hafnium isotopes were analysed using a Nu Instruments Plasma HR MC–ICPMS at PCIGR. For Lu, isobaric interference of ^{176}Yb on ^{176}Lu was corrected using an exponential correlation of $^{176}Yb/^{171}Yb$ and $^{174}Yb/^{171}Yb$, calibrated through replicate analyses of NIST Yb solution standards at different concentrations (10–100 ppb)[107] and using Yb isotope abundances[108]. For Hf, ^{180}Ta and ^{180}W isobaric interferences on ^{180}Hf were corrected for through analysis of mass over charge corresponding to ^{181}Ta and ^{183}W and applying a Hf-based mass bias. Mass bias corrections were calculated using an exponential law and assuming $^{179}Hf/^{177}Hf = 0.7325$ (Hf, Ta, W) and $^{173}Yb/^{171}Yb = 1.1296$ (Lu, Yb). External reproducibility of $^{176}Hf/^{177}Hf$ was estimated by comparing internal and external uncertainty for replicate analyses of JMC-475 and ATI-475—isotopically identical to JMC-475 and made from the same metal ingots as the original JMC-475—

done at concentrations that bracketed those of samples (5–50 ppb)[109]. The external $^{176}Hf/^{177}Hf$ reproducibility (2σ) of the replicate standard analyses was 0.3 εHf during the analytical sessions. Isochrons were constructed using $\lambda176Lu = 1.867 \times 10–11$ yr-1[110,111]. Uncertainties are cited at the 2σ level. The Lu–Hf data are in Supplementary Data Table S5.

Monte Carlo simulations

Two- to three-variable mixtures of mantle-derived magma, water (seawater, meteoric water), crustal assimilants, basaltic protolith and externally-derived melt were modelled using Monte Carlo simulations to compare each model to observed garnet and zircon $\delta^{18}O$ ranges.

We use the following as end-members, all of which are derived from published reservoirs or our new data. All the parameters and equations are summarised in Supplementary Data Table S6.

1. Mantle-derived $\delta^{18}O$ is 5.3 ± 0.6 ‰ (Gaussian distribution), which is shown to be highly homogeneous through time and space owing to this primordial reservoir being the predominant oxygen component on Earth[32].
2. Seawater $\delta^{18}O$ is modelled as 0^{+3}_{-1} ‰ (triangular distribution), which assumes that seawater oxygen isotopic compositions have stayed essentially invariant since the Archaean[58,59]. Until recently, this has been controversial, with suggestions that Archaean and Proterozoic seawater had significantly lower $\delta^{18}O$ (by 10 ‰ or more) based on low-$\delta^{18}O$ marine cherts and carbonates[112]. However, evidence from 2 Ga ophiolites[113], 3.8 Ga serpentine minerals[114], Archaean pillow basalts[115] kerogens in Archaean chert[116] and triple O isotopic data[117] have shown that low-$\delta^{18}O$ Precambrian chemical sedimentary rocks are a function of warmer sea surface temperatures (near the equator) and post-depositional meteoric alteration.
3. Meteoric water is modelled with a $\delta^{18}O$ of -10^{+10}_{-20} ‰ (triangular distribution). Through time, meteoric water has always been broadly equal to or more negative than seawater throughout Earth's history. However, meteoric water is geographically highly variable as a function of climate (temperature and rainfall)[118]. Our broad range of -10^{+10}_{-20} ‰ encapsulates all but the most arid and polar conditions[118], consistent with paleomagnetic data that indicate proto-Northern Australia was located between 20 and 60°N latitude between 1800 and 1400 Ma.
4. Crustal contaminants have $\delta^{18}O$ of 15^{+15}_{-5} ‰ (triangular distribution), which includes the compositions of present-day to Archaean marine clastic sediments, pelagic clays and carbonates[31]. Whilst there is undoubtedly spatial variability of these isotopic reservoirs in the Precambrian, as there is with the present-day distribution of these sediments, this wide but positive $\delta^{18}O$ captures the expected spectrum.

Each end-member component has two parameters (Supplementary Data Table S6): (a) distribution of $\delta^{18}O$, recalculated to absolute $^{18}O/^{16}O$ and (b) atomic proportion of O_2 within the rock. The probability distributions for $\delta^{18}O$ are either Gaussian (i.e., normal) or triangular (minimum and maximum, with a mode that controls the skew of the triangle). The ratio between the two parameters is also important, and these are modelled as either triangular or gamma (similar to logarithmic but with variable shape and scale parameters). The values used for the distributions are listed in the Main text and detailed in Supplementary Data Table S6.

An important variable is the amount of O in the different end-members, which depends on the atomic proportions of O_2 to other elements for each of the reacting minerals or phases. Both waters (H_2O) are relatively straightforward at 33 % O_2, and these are kept fixed. Mantle-derived magma and crustal assimilants could range from 33 % (quartz, SiO_2) to 43 % (olivine, $[Mg, Fe]_2SiO_4$), and this range is used for both. For mantle-derived magma, a mean of 41.5 % O_2 was chosen for a typical peridotite that comprises even proportions of orthopyroxene ($[Fe, Mg]_2Si_2O_6$, 40% O_2) and olivine (43 % O_2). For crustal assimilants, which are most likely sedimentary detritus eroded from more evolved rocks (e.g. TTGs), we use a mean of 35 % O_2 for a typical tonalite that comprises even proportions of quartz (33% O_2) and Ca-rich plagioclase ($CaAl_2Si_2O_8$, 38% O_2).

Article

The Monte Carlo simulations were performed using the Excel add-on programme QuantumXL, for 10,000 trials in native mode using a Mersenne Twister pseudo-random number generator based on the user-defined probability distributions. The following calculations were performed (detailed in Supplementary Data Table S6):

- Scenario 1: Mantle-derived magma contaminated with seawater or meteoric water;
- Scenario 2: Mantle-derived magma contaminated with various proportions of crustal (sedimentary) assimilants;
- Scenario 3: Basaltic protolith melt with external, mantle-derived (±crustally-contaminated) melt.

After 10,000 trials, histograms of output values are generated, showing the distribution of computed $\delta^{18}O$, quoted at 95% confidence (similar to 2σ but allowing for a skewed distribution, Fig. 3). These histograms represent the probability distribution of the true range of the variables calculated using the Monte Carlo simulations and can be directly compared to the observed zircon and garnet $\delta^{18}O$ record (Fig. 2).

Data availability

References

1. Collins, W. J., Murphy, J. B., Johnson, T. E. & Huang, H.-Q. Critical role of water in the formation of continental crust. *Nat. Geosci.* **13**, 331–338 (2020).
2. Bea, F. The sources of energy for crustal melting and the geochemistry of heat-producing elements. *Lithos* **153**, 278–291 (2012).
3. Clemens, J. D., Stevens, G. & Bryan, S. E. Conditions during the formation of granitic magmas by crustal melting–hot or cold; drenched, damp or dry?. *Earth Sci. Rev.* **200**, 102982 (2020).
4. Volante, S. et al. Reassessing zircon-monazite thermometry with thermodynamic modelling: insights from the Georgetown igneous complex, NE Australia. *Contrib. Miner. Petrol.* **175**, (2020). 110.
5. Collins, W. J., Murphy, J. B., Blereau, E. & Huang, H. Q. Water availability controls crustal melting temperatures. *Lithos* **402**, 106351 (2021).
6. Schwindinger, M., Weinberg, R. F. & Clos, F. Wet or dry? The difficulty of identifying the presence of water during crustal melting. *J. Metamorphic Geol.* **37**, 339–358 (2019).
7. Sawyer, E. W. Migmatites formed by water-fluxed partial melting of a leucogranodiorite protolith: microstructures in the residual rocks and source of the fluid. *Lithos* **116**, 273–286 (2010).
8. Dhuime, B., Hawkesworth, C. J., Cawood, P. A. & Storey, C. D. A change in the geodynamics of continental growth 3 billion years ago. *Science* **335**, 1334–1336 (2012).
9. Weinberg, R. F. & Hasalová, P. Water-fluxed melting of the continental crust: a review. *Lithos* **212**, 158–188 (2015).
10. Collins, W. J., Huang, H. -Q. & Jiang, X. Water-fluxed crustal melting produces Cordilleran batholiths. *Geology* **44**, 143–146 (2016).
11. Wang, X., et al. Adakite generation as a result of fluid-fluxed melting at normal lower crustal pressures. *Earth Planet. Sci. Lett.* **594**, 117744 (2022).
12. Grove, T. L., Till, C. B. & Krawczynski, M. J. The role of H2O in subduction zone magmatism. *Annu. Rev. Earth Planet. Sci.* **40**, 413–439 (2012).
13. Tuttle, O. F. & Bowen, N. L. (eds) *Origin of Granite in the Light of Experimental Studies in the System NaAlSi₃O₈–KAlSi₃O₈–SiO₂–H₂O* (Geological Society of America, 1958).
14. Zhu, K. -Y., Li, Z. -X., Xu, X. -S. & Wilde, S. A. A Mesozoic Andean-type orogenic cycle in southeastern China as recorded by granitoid evolution. *Am. J. Sci.* **314**, 187–234 (2014).
15. Pourteau, A. et al. TTG generation by fluid-fluxed crustal melting: direct evidence from the Proterozoic Georgetown Inlier, NE Australia. *Earth Planet. Sci. Lett.* **550**, 116548 (2020).
16. Schorn, S., Hartnady, M. I. H., Diener, J. F. A., Clark, C. & Harris, C. H2O-fluxed melting of eclogite during exhumation: an example from the eclogite type-locality, Eastern Alps (Austria). *Lithos* **390–391**, 106118 (2021).
17. Rubatto, D., Hermann, J., Berger, A. & Engi, M. Protracted fluid-induced melting during Barrovian metamorphism in the Central Alps. *Contrib. Miner. Petrol.* **158**, 703–722 (2009).
18. Schmidt, M. W. & Poli, S. Experimentally based water budgets for dehydrating slabs and consequences for arc magma generation. *Earth Planet. Sci. Lett.* **163**, 361–379 (1998).
19. Yang, C. -M. et al. High water contents in zircons suggest water-fluxed crustal melting during cratonic destruction. *Geophys. Res. Lett.* **49**, e2021GL097126 (2022).
20. Prent, A. M., et al. Apatite and monazite: an effective duo to unravel superimposed fluid-flow and deformation events in reactivated shear zones. *Lithos* **376–377**, 105752 (2020).
21. Ferrero, S. et al. Embryos of TTGs in Gore Mountain garnet megacrysts from water-fluxed melting of the lower crust. *Earth Planet. Sci. Lett.* **569**, (2021). 117058.
22. Arndt, N. How did the continental crust form: no basalt, no water, no granite. *Precambrian Res.* **397**, 107196 (2023).
23. Wu, Z., Song, J., Zhao, G. & Pan, Z. Water-induced mantle overturns leading to the origins of archean continents and subcontinental lithospheric mantle. *Geophys. Res. Lett.* **50**, e2023GL105178 (2023).
24. Smithies, R. H. et al. Oxygen isotopes trace the origins of Earth's earliest continental crust. *Nature* **592**, 70–75 (2021).
25. Johnson, T. E. et al. Giant impacts and the origin and evolution of continents. *Nature* **608**, 330–335 (2022).
26. Hernández-Montenegro, J. D., Palin, R. M., Zuluaga, C. A. & Hernández-Uribe, D. Archean continental crust formed by magma hybridization and voluminous partial melting. *Sci. Rep.* **11**, 1–9 (2021).
27. Daczko, N. R., Piazolo, S., Meek, U., Stuart, C. A. & Elliott, V. Hornblendite delineates zones of mass transfer through the lower crust. *Sci. Rep.* **6**, (2016). 31369.
28. GARRIDO, C. J. et al. Petrogenesis of mafic garnet granulite in the lower crust of the Kohistan paleo-arc complex (Northern Pakistan): implications for intra-crustal differentiation of island arcs and generation of continental crust. *J. Petrol.* **47**, 1873–1914 (2006).
29. Johnson, T. E. et al. Secular change in TTG compositions: implications for the evolution of Archaean geodynamics. *Earth Planet. Sci. Lett.* **505**, 65–75 (2019).
30. Bindeman, I. Oxygen isotopes in mantle and crustal magmas as revealed by single crystal analysis. *Rev. Miner. Geochem.* **69**, 445–478 (2008).
31. Eiler, J. M. Oxygen isotope variations of basaltic lavas and upper mantle rocks. *Rev. Miner. Geochem.* **43**, 319–364 (2001).
32. Valley, J. W. et al. 4.4 billion years of crustal maturation: oxygen isotope ratios of magmatic zircon. *Contrib. Miner. Petrol.* **150**, 561–580 (2005).
33. Watson, E. B. & Cherniak, D. J. Oxygen diffusion in zircon. *Earth Planet. Sci. Lett.* **148**, 527–544 (1997).
34. Scicchitano, M. R. et al. Oxygen diffusion in garnet: experimental calibration and implications for timescales of metamorphic processes and retention of primary O isotopic signatures. *Am. Mineralogist. J. Earth Planet. Mater.* **107**, 1425–1441 (2022).
35. Hiess, J., Bennett, V. C., Nutman, A. P. & Williams, I. S. Archaean fluid-assisted crustal cannibalism recorded by low δ18O and negative εHf(T) isotopic signatures of West Greenland granite zircon. *Contrib. Miner. Pet.* **161**, 1027–1050 (2011).

36. Kirkland, C. L. et al. Bimodality in zircon oxygen isotopes and implications for crustal melting on the early Earth. *Earth Planet. Sci. Lett.* **625**, (2024). 118491.

37. Gamaleldien, H. et al. Onset of the Earth's hydrological cycle four billion years ago or earlier. *Nat. Geosci.* **17**, 560–565 (2024).

38. Valley, J. W., Kita, N. T. & Fayek, M. In situ oxygen isotope geochemistry by ion microprobe. *MAC Short. Course. Secondary Ion. Mass Spectrom. Earth Sci.* **41**, 19–63 (2009).

39. Riches, A. J. V. et al. In situ oxygen-isotope, major-, and trace-element constraints on the metasomatic modification and crustal origin of a diamondiferous eclogite from Roberts Victor, Kaapvaal Craton. *Geochim. Et. Cosmochim. Acta* **174**, 345–359 (2016).

40. Bovay, T., Rubatto, D. & Lanari, P. Pervasive fluid-rock interaction in subducted oceanic crust revealed by oxygen isotope zoning in garnet. *Contrib. Miner. Petrol.* **176**, 1–22 (2021).

41. Fan, G. -H., et al. Garnet secondary ion mass spectrometry oxygen isotopes reveal crucial roles of pulsed magmatic fluid and its mixing with meteoric water in lode gold genesis. *Proc. Natl. Acad. Sci. USA* **119**, e2116380119 (2022).

42. Hammerli, J., Kemp, A. I. S. & Jeon, H. An Archean Yellowstone? Evidence from extremely low $\delta18O$ in zircons preserved in granulites of the Yilgarn Craton, Western Australia. *Geology* **46**, 411–414 (2018).

43. Petersson, A., Waight, T., Kemp, A. I. S., Whitehouse Martin, J. & Valley, J. W. An Eoarchean continental nucleus for the Fennoscandian Shield and a link to the North Atlantic craton. *Geology* **52**, 171–175 (2023).

44. Volante, S. et al. Spatio–temporal evolution of Mesoproterozoic magmatism in NE Australia: a hybrid tectonic model for final Nuna assembly. *Precambrian Res.* **372**, (2022). 106602.

45. Baker, M. J., Crawford, A. J. & Withnall, I. W. Geochemical, Sm–Nd isotopic characteristics and petrogenesis of Paleoproterozoic mafic rocks from the Georgetown Inlier, north Queensland: implications for relationship with the Broken Hill and Mount Isa Eastern Succession. *Precambrian Res.* **177**, 39–54 (2010).

46. Black, L. P., Gregory, P., Withnall, I. W. & Bain, J. H. C. U–Pb zircon age for the Etheridge Group, Georgetown region, north Queensland: implications for relationship with the Broken Hill and Mt Isa sequences*. *Aust. J. Earth Sci.* **45**, 925–935 (1998).

47. Pourteau, A. et al. 1.6 Ga crustal thickening along the final Nuna suture. *Geology* **46**, 959–962 (2018).

48. Volante, S. et al. Multiple P–T–d–t paths reveal the evolution of the final Nuna assembly in northeast Australia. *J. Metamorphic Geol.* **38**, 593–627 (2020).

49. Boger, S. D. & Hansen, D. Metamorphic evolution of the Georgetown Inlier, northeast Queensland, Australia; evidence for an accreted Palaeoproterozoic terrane?. *J. Metamorphic Geol.* **22**, 511–527 (2004).

50. Nordsvan, A. R. et al. Post-collisional magmatism in NE Australia during Mesoproterozoic supercontinent Nuna: insights from new zircon UPb and LuHf data. *Lithos* **428–429**, (2022):106827.

51. Volante, S. et al. Structural evolution of a 1.6 Ga orogeny related to the final assembly of the supercontinent Nuna: coupling of episodic and progressive deformation. *Tectonics* **39**, e2020TC006162 (2020).

52. Olierook, H. K. H. et al. Mineralization proximal to the final Nuna suture in northeastern Australia. *Gondwana Res.* **92**, 54–71 (2021).

53. Hills, Q. *Deformational and metamorphic history of the Georgetown Inlier, North Queensland implications for the 1.7 to 1.5 Ga tectonic evolution of northeastern Proterozoic Australia* (Monash University, 2004, 2003).

54. Valley, J. W. Oxygen isotopes in zircon. *Rev. Miner. Geochem.* **53**, 343–385 (2003).

55. Valley, J. W., Bindeman, I. N. & Peck, W. H. Empirical calibration of oxygen isotope fractionation in zircon. *Geochim. Et. Cosmochim. Acta* **67**, 3257–3266 (2003).

56. Martin, L. A. et al. Garnet oxygen analysis by SHRIMP-SI: matrix corrections and application to high-pressure metasomatic rocks from Alpine Corsica. *Chem. Geol.* **374**, 25–36 (2014).

57. Vho, A., Rubatto, D., Putlitz, B. & Bouvier, A. -S. New reference materials and assessment of matrix effects for SIMS measurements of oxygen isotopes in garnet. *Geostand. Geoanal. Res.* **44**, 459–471 (2020).

58. Liljestrand, F. L., et al. The triple oxygen isotope composition of Precambrian chert. *Earth Planet. Sci. Lett.* **537**, 116167 (2020).

59. Lécuyer, C. & Allemand, P. Modelling of the oxygen isotope evolution of seawater: implications for the climate interpretation of the δ18O of marine sediments. *Geochim. Et. Cosmochim. Acta* **63**, 351–361 (1999).

60. Bindeman, I. N., Bekker, A. & Zakharov, D. O. Oxygen isotope perspective on crustal evolution on early Earth: a record of Precambrian shales with emphasis on Paleoproterozoic glaciations and Great Oxygenation Event. *Earth Planet. Sci. Lett.* **437**, 101–113 (2016).

61. Hopkinson, T. N. et al. The identification and significance of pure sediment-derived granites. *Earth Planet. Sci. Lett.* **467**, 57–63 (2017).

62. Bucholz, C. E. & Hernández-Montenegro, J. D. Temporal variation in oxygen isotopes of peraluminous granites derived from sedimentary sources. *Lithos* **492–493**, 107864 (2025).

63. Appleby, S. K. et al. Do S-type granites commonly sample infracrustal sources? New results from an integrated O, U–Pb and Hf isotope study of zircon. *Contrib. Miner. Pet.* **160**, 115–132 (2010).

64. Villaros, A., Buick, I. & Stevens, G. Isotopic variations in S-type granites: an inheritance from a heterogeneous source?. *Contrib. Miner. Petrol.* **163**, 243–257 (2012).

65. Cavosie, A. J. et al. The origin of high δ18O zircons: marbles, megacrysts, and metamorphism. *Contrib. Miner. Pet.* **162**, 961–974 (2011).

66. Muehlenbachs, K. The oxygen isotopic composition of the oceans, sediments and the seafloor. *Chem. Geol.* **145**, 263–273 (1998).

67. Kasting, J. F. et al. Paleoclimates, ocean depth, and the oxygen isotopic composition of seawater. *Earth Planet. Sci. Lett.* **252**, 82–93 (2006).

68. Perry, E. C. The oxygen isotope chemistry of ancient cherts. *Earth Planet. Sci. Lett.* **3**, 62–66 (1967).

69. Lécuyer, C., Bojar, A.-V., Daux, V. & Legendre, S. Geographic variations in the slope of the δ^2H–$\delta^{18}O$ meteoric water line over Europe: a record of increasing continentality. *Geol. Soc. Lond. Spec. Publ.* **507**, 5–17 (2021).

70. Collins, W. J. Lachlan Fold Belt granitoids: products of three-component mixing. *Earth Environ. Sci. Trans. R. Soc. Edinb.* **87**, 171–181 (1996).

71. Kemp, A. et al. Magmatic and crustal differentiation history of granitic rocks from Hf-O isotopes in zircon. *Science* **315**, 980–983 (2007).

72. Spencer, C. J., et al. Disparities in oxygen isotopes of detrital and igneous zircon identify erosional bias in crustal rock record. *Earth Planet. Sci. Lett.* **577**, 117248 (2022).

73. Valley, J. W., Kinny, P. D., Schulze, D. J. & Spicuzza, M. J. Zircon megacrysts from kimberlite: oxygen isotope variability among mantle melts. *Contrib. Miner. Pet.* **133**, 1–11 (1998).

74. Nordsvan, A. R. et al. Laurentian crust in northeast Australia: Implications for the assembly of the supercontinent Nuna. *Geology* **46**, 251–254 (2018).

75. Li, J., et al. Heterogeneous exhumation of the Mount Isa orogen in NE Australia after 1.6 Ga nuna assembly: new high-precision 40Ar/39Ar thermochronological constraints. *Tectonics* **39**, e2020TC006129 (2020).

76. Spencer, C. J., Mitchell, R. N. & Brown, M. Enigmatic Mid-Proterozoic Orogens: Hot, Thin, and Low. *Geophys. Res. Lett.* **48**, e2021GL093312 (2021).

77. Korsch, R. J. et al. Crustal architecture and geodynamics of North Queensland, Australia: Insights from deep seismic reflection profiling. *Tectonophysics* **572–573**, 76–99 (2012).

78. Jolivet, L. et al. The geological signature of a slab tear below the Aegean. *Tectonophysics* **659**, 166–182 (2015).

79. Nordsvan, A. R. *Sedimentology and provenance of NE Australian Proterozoic basins with relevance to the formation of the Supercontinent Nuna*. School of Earth and Planetary Sciences, Curtin University, *Perth* 217 (2020).

80. Betts, P. G. et al. Mesoproterozoic plume-modified orogenesis in eastern Precambrian Australia. *Tectonics* https://doi.org/10.1029/2008TC002325 (2009).

81. Murgulov, V. et al. Crustal evolution in the Georgetown Inlier, North Queensland, Australia: a detrital zircon grain study. *Chem. Geol.* **245**, 198–218 (2007).

82. Gerya, T. Precambrian geodynamics: concepts and models. *Gondwana Res.* **25**, 442–463 (2014).

83. Sizova, E., Gerya, T. & Brown, M. Contrasting styles of Phanerozoic and Precambrian continental collision. *Gondwana Res.* **25**, 522–545 (2014).

84. Hartnady, M. I. et al. Fluid processes in the early Earth and the growth of continents. *Earth Planet. Sci. Lett.* **594**, 117695 (2022).

85. Palin, R. M. & White, R. W. Emergence of blueschists on Earth linked to secular changes in oceanic crust composition. *Nat. Geosci.* **9**, 60–64 (2016).

86. Starr, P. G. & Pattison, D. R. M. Metamorphic devolatilization of basalts across the greenschist-amphibolite facies transition zone: insights from isograd mapping, petrography and thermodynamic modelling. *Lithos* **342–343**, 295–314 (2019).

87. Tamblyn, R., et al. Hydrated komatiites as a source of water for TTG formation in the Archean. *Earth Planet. Sci. Lett.* **603**, 117982 (2023).

88. Gurenko, A. A., Kamenetsky, V. S. & Kerr, A. C. Oxygen isotopes and volatile contents of the Gorgona komatiites, Colombia: a confirmation of the deep mantle origin of H2O. *Earth Planet. Sci. Lett.* **454**, 154–165 (2016).

89. Smit, M. A., Musiyachenko, K. A. & Goumans, J. Archaean continental crust formed from mafic cumulates. *Nat. Commun.* **15**, 692 (2024).

90. Król, P., Kusiak, M. A., Whitehouse, M. J., Dunkley, D. J. & Wilde, S. A. Eoarchean low δ18O zircon indicates emergent land at 3.73 Ga. *Precambrian Res.* **408**, 107416 (2024).

91. Horstwood, M. S. A. et al. Community-Derived Standards for LA-ICP-MS U–(Th–)Pb Geochronology - Uncertainty Propagation, Age Interpretation and Data Reporting. *Geostand. Geoanal. Res.* **40**, 311–332 (2016).

92. Jackson, S. E., Pearson, N. J., Griffin, W. L. & Belousova, E. A. The application of laser ablation-inductively coupled plasma-mass spectrometry to in situ U–Pb zircon geochronology. *Chem. Geol.* **211**, 47–69 (2004).

93. Stern, R. A., Bodorkos, S., Kamo, S. L., Hickman, A. H. & Corfu, F. Measurement of SIMS instrumental mass fractionation of Pb isotopes during zircon dating. *Geostand. Geoanal. Res.* **33**, 145–168 (2009).

94. Sláma, J. et al. Plešovice zircon—a new natural reference material for U–Pb and Hf isotopic microanalysis. *Chem. Geol.* **249**, 1–35 (2008).

95. Wiedenbeck, M. et al. Three natural zircon standards for U-Th-Pb, Lu-Hf, trace element and REE analyses. *Geostand. Newsl.* **19**, 1–23 (1995).

96. Marsh, J., Jørgensen, T., Petrus, J., Hamilton, M. & Mole, D. U–Pb, trace element, and hafnium isotope composition of the Maniitsoq zircon: a potential new Archean zircon reference material. *Goldschmidt Abstr.* **2161**, 2019 (2019).

97. Paton, C., Hellstrom, J., Paul, B., Woodhead, J. & Hergt, J. Iolite: freeware for the visualisation and processing of mass spectrometric data. *J. Anal. At. Spectrom.* **26**, 2508–2518 (2011).

98. Vermeesch, P. IsoplotR: a free and open toolbox for geochronology. *Geosci. Front.* **9**, 1479–1493 (2018).

99. Spencer, C. J., Kirkland, C. L. & Taylor, R. J. M. Strategies towards statistically robust interpretations of in situ U–Pb zircon geochronology. *Geosci. Front.* **7**, 581–589 (2016).

100. Wiedenbeck, M. et al. Further characterisation of the 91500 zircon crystal. *Geostand. Geoanal. Res.* **28**, 9–39 (2004).

101. Petersson, A. et al. A new 3.59 Ga magmatic suite and a chondritic source to the east Pilbara Craton. *Chem. Geol.* **511**, 51–70 (2019).

102. Valley, J. W., Kitchen, N., Kohn, M. J., Niendorf, C. R. & Spicuzza, M. J. UWG-2, a garnet standard for oxygen isotope ratios: Strategies for high precision and accuracy with laser heating. *Geochim. Et. Cosmochim. Acta* **59**, 5223–5231 (1995).

103. Vielzeuf, D., Champenois, M., Valley, J. W., Brunet, F. & Devidal, J. L. SIMS analyses of oxygen isotopes: matrix effects in Fe–Mg–Ca garnets. *Chem. Geol.* **223**, 208–226 (2005).

104. Page, F. Z., Kita, N. T. & Valley, J. W. Ion microprobe analysis of oxygen isotopes in garnets of complex chemistry. *Chem. Geol.* **270**, 9–19 (2010).

105. Cutts, J. A. & Smit, M. A. Rates of deep continental burial from Lu-Hf garnet chronology and Zr-in-rutile thermometry on (Ultra)high-pressure rocks. *Tectonics* **37**, 71–88 (2018).

106. Münker, C., Weyer, S., Scherer, E. & Mezger, K. Separation of high field strength elements (Nb, Ta, Zr, Hf) and Lu from rock samples for MC-ICPMS measurements. *Geochem. Geophys. Geosyst.* https://doi.org/10.1029/2001GC000183 (2001).

107. Blichert-Toft, J., Boyet, M., Télouk, P. & Albarède, F. 147Sm–143Nd and 176Lu–176Hf in eucrites and the differentiation of the HED parent body. *Earth Planet. Sci. Lett.* **204**, 167–181 (2002).

108. Vervoort, J. D., Patchett, P. J., Söderlund, U. & Baker, M. Isotopic composition of Yb and the determination of Lu concentrations and Lu/Hf ratios by isotope dilution using MC-ICPMS. *Geochem. Geophys. Geosyst.* https://doi.org/10.1029/2004GC000721 (2004).

109. Bizzarro, M., Baker, J. A., Haack, H., Ulfbeck, D. & Rosing, M. Early history of Earth's crust–mantle system inferred from hafnium isotopes in chondrites. *Nature* **421**, 931–933 (2003).

110. Scherer, E., Münker, C. & Mezger, K. Calibration of the lutetium-hafnium clock. *Science* **293**, 683–687 (2001).

111. Söderlund, U., Patchett, P. J., Vervoort, J. D. & Isachsen, C. E. The 176 Lu decay constant determined by Lu–Hf and U–Pb isotope systematics of Precambrian mafic intrusions. *Earth Planet. Sci. Lett.* **219**, 311–324 (2004).

112. Jaffrés, J. B. D., Shields, G. A. & Wallmann, K. The oxygen isotope evolution of seawater: a critical review of a long-standing controversy and an improved geological water cycle model for the past 3.4 billion years. *Earth Sci. Rev.* **83**, 83–122 (2007).

113. Holmden, C. & Muehlenbachs, K. The 18O/16O ratio of 2-billion-year-old seawater inferred from ancient oceanic crust. *Science* **259**, 1733–1736 (1993).

114. Pope, E. C., Bird, D. K. & Rosing, M. T. Isotope composition and volume of Earth's early oceans. *Proc. Natl. Acad. Sci. USA* **109**, 4371–4376 (2012).

115. O'Neil, J. R. & Truesdell, A. H. Oxygen isotope fractionation studies of solute-water interactions. *Geochem. Soc. Spec. Publ.* **3**, 17–25 (1991).

116. Tartèse, R., Chaussidon, M., Gurenko, A., Delarue, F. & Robert, F. Warm Archean oceans reconstructed from oxygen isotope composition of early-life remnants. *Geochem. Perspect. Lett.* **3**, 55–65 (2017).

117. McGunnigle, J. et al. Triple oxygen isotope evidence for a hot Archean ocean. *Geology* **50**, 991–995 (2022).

118. Putman, A. L., Fiorella, R. P., Bowen, G. J. & Cai, Z. A global perspective on local meteoric water lines: Meta-analytic insight into fundamental controls and practical constraints. *Water Resour. Res.* **55**, 6896–6910 (2019).

Author contributions
S.V., A. P., Z.-X. Li and W. J. C. designed the study and collected the samples. S.V. and A. P. drafted the figures. L.S.D. collected zircon CL images and geochronology data. H.K.H. O. collected and processed the zircon geochronology data and performed the quantitative modelling. L.M. collected and processed SIMS oxygen isotope data. M.S. collected and processed garnet geochronology data. S.V. led the writing of the manuscript with contributions from all authors.

Competing interests
The authors declare no competing interests.

Additional information
Supplementary information The online version contains supplementary material available at https://doi.org/10.1038/s43247-025-02250-z.

Correspondence and requests for materials should be addressed to Silvia Volante.

Peer review information *Communications Earth & Environment* thanks Xiaoping Xia and the other anonymous reviewer(s) for their contribution to the peer review of this work. Primary Handling Editors: David Hernández Uribe and Carolina Ortiz Guerrero. A peer review file is available.

Reprints and permissions information is available at http://www.nature.com/reprints

Publisher's note Springer Nature remains neutral with regard to jurisdictional claims in published maps and institutional affiliations.